THE GEOLOGICAL SOCIETY OF AMERICA®

Metallogenic fingerprint of a metasomatized lithospheric mantle feeding gold endowment in the western Mediterranean basin

Erwin Schettino[1,2,†], Claudio Marchesi[1,2], José María González-Jiménez[1,2], Edward Saunders[3], Károly Hidas[4], Fernando Gervilla[1,2], and Carlos J. Garrido[1]

[1]*Instituto Andaluz de Ciencias de la Tierra, Consejo Superior de Investigaciones Científicas-Universidad de Granada, Avenida de las Palmeras 4, 18100 Armilla, Spain*

[2]*Departamento de Mineralogía y Petrología, Universidad de Granada, Avenida Fuentenueva s/n, 18002 Granada, Spain*

[3]*Division of Earth Sciences, School of Environmental and Rural Science, University of New England, Armidale, NSW 2350, Australia*

[4]*Departamento de Investigación y Prospectiva Geocientífica, Instituto Geológico y Minero de España, Calle de la Calera 1, 28760 Tres Cantos, Spain*

ABSTRACT

Spinel peridotite xenoliths (one plagioclase-bearing) hosted in alkaline basalts from Tallante (southeast Spain) record the mineralogical and geochemical fingerprint of the subcontinental lithospheric mantle (SCLM) evolution beneath the southern Iberian margin. Mantle metasomatism in fertile lherzolites caused the crystallization of clinopyroxene + orthopyroxene + spinel clusters through the percolation of Miocene subalkaline melts during the westward migration of the subduction front in the western Mediterranean. In the Pliocene, heat and volatiles provided by alkaline host-magmas triggered very low melting degrees of metasomatic pyroxene-spinel assemblages, producing melt quenched to silicate glass and reactive spongy coronae around clinopyroxene and spinel. Refertilization of the Tallante peridotites induced the precipitation of base-metal sulfides (BMS) included in metasomatic clino- and orthopyroxene. These sulfides consist of pentlandite ± chalcopyrite ± bornite aggregates with homogeneous composition in terms of major elements (Ni, Fe, Cu) and semi-metals (Se, As, Te, Sb, Bi), but with wide variability of platinum-group elements (PGE) fractionation ($0.14 < Pd_N/Ir_N < 30.74$). Heterogeneous PGE signatures, as well as the presence of euhedral Pt-Pd-Sn-rich platinum-group minerals (PGM) and/or Au-particles within BMS, cannot be explained by conventional models of chalcophile partitioning from sulfide melt. Alternatively, we suggest that they reflect the incorporation of distinct populations of BMS, PGM, and metal nanoparticles (especially of Pt, Pd, and Au) during mantle melting and/or melt percolation. Therefore, we conclude that Miocene subalkaline melts released by asthenosphere upwelling upon slab tearing of the Iberian continental margin effectively stored metals in metasomatized domains of this sector of the SCLM. Remarkably high Au concentrations in Tallante BMS (median 1.78 ppm) support that these metasomatized domains provided a fertile source of metals, especially gold, for the ore-productive Miocene magmatism of the westernmost Mediterranean.

INTRODUCTION

Accretionary orogens host a wide range of magmatic and hydrothermal ore deposits that provide the world's largest resource of copper, gold, and silver, as well as significant reserves of base metals, such as zinc, lead, iron, tin, and molybdenum (Bierlein et al., 2009; Groves et al., 2020). These ore deposits are the foci of large-scale systems of mass and energy flux, where extremely efficient geological processes concentrate metals in a small volume of rock (Hronsky et al., 2012), thus producing deposits of economic interest. The whole process of ore mineralization usually requires a scale-integrated combination of factors and mechanisms acting from mantle depths to shallow crust, including a fertile source of metals, a focused fluid/melt flow capable of mobilizing the metal cargoes, and a geochemical trap in the upper crust that favors the selective precipitation of anomalous amounts of metals (Richards, 2013).

During the last decade, an ever-increasing number of works have documented the key-role of mantle magmas in the formation of magmatic-hydrothermal ores in the crust (e.g., Richards, 2009; Holwell et al., 2019; Blanks et al., 2020; Rabayrol and Hart, 2021). The generation of ore-productive magmas is related to the existence of specific metal-rich sources in the subcontinental lithospheric mantle (SCLM), ranging in size from micrometer- to terrane-scales (McInnes et al., 1999; Griffin et al., 2013; Tassara et al., 2017; Holwell et al., 2019; Wang et al., 2020; Chong et al., 2021). In these domains, metals are mostly concentrated in base-metal sulfides (BMS), nano-to-micrometer-sized platinum-group minerals (PGM), and native alloys. These minerals actually constitute the main repositories of noble metals (platinum-group elements, PGE: Ru, Rh, Pd, Os, Ir, and Pt, plus Au) and semi-metals (Se, As, Te, Bi, Sb, Sn) in the mantle due to the strong chalcophile and siderophile affinities of these elements (Alard et al., 2000; Luguet et al., 2001; Lorand et al., 2008; O'Driscoll and González-Jiménez, 2016). The response of BMS, PGM, and native alloys to partial melting and mantle metasomatism normally involves re-working of the metal inventory of the mantle (Aulbach et al., 2016; Lorand and Luguet, 2016; González-Jiménez et al., 2020). For instance, melting and percolation of sulfide-undersaturated silicate melts at increasing melt/rock ratios favor the progressive removal of BMS and exsolution of residual laurite/Pt-Ir-Os alloys (Peregoedova et al., 2004; Luguet et al., 2007; Lorand et al., 2010), coupled with a general depletion of incompatible Pd-group PGE (P-PGE: Pd, Pt) in the bulk rock (Wang et al., 2009; Lorand et al., 2013; Saunders et al., 2015). On the other hand, mantle metasomatism at decreasing melt/rock ratios typically drives the precipitation of Ni-Cu-rich BMS and bismuth-otellurides/arsenides enriched in Pd, Pt, Rh, and

Erwin Schettino https://orcid.org/0000-0002-3606-8854

[†]eschettino@correo.ugr.es.

GSA Bulletin;
Published online 20 September 2021

https://doi.org/10.1130/B36065.1; 14 figures; 1 supplemental file.

Au (Alard et al., 2000, 2011; Lorand and Alard, 2001; Luguet et al., 2003; González-Jiménez et al., 2020). Therefore, several studies have used the variability of PGE and semi-metals systematics in distinct populations of BMS and PGM as geochemical markers for assessing the mobility of metals in the mantle, and thus the metallogenic fertility of the SCLM (González-Jiménez et al., 2014, 2019, 2020; Saunders et al., 2015, 2016; Hughes et al., 2017; Tassara et al., 2018).

Peridotite xenoliths rapidly brought to the surface by volcanic activity provide exceptional information about the mantle source of metal-rich magmas, as they usually preserve the mineralogical-geochemical fingerprint of the mechanisms and/or agents that control the mobility and storage of metals in the SCLM. For instance, peridotite xenoliths from the giant Ladolam Au deposit (Papua New Guinea) record the contribution of the metasomatized sub-arc mantle to the gold-inventory of the ores (McInnes et al., 1999). Furthermore, gold-rich (and precious metals-rich) BMS in peridotite xenoliths from southern Patagonia document how refertilization by plume-derived melts generated a gold-fertile mantle source beneath the auriferous province of the Deseado Massif (Tassara et al., 2017). However, despite these examples supporting the mantle-inheritance of the metal budget of crustal ore deposits, many other ore-systems lack any direct evidence of mantle contribution. Moreover, BMS and PGM data of peridotite xenoliths from ore-productive regional settings are still scarce and, therefore, the melt-rock reaction processes by which the SCLM may be enriched in noble and/or semi-metals are still poorly constrained.

The peridotite xenoliths hosted in the alkali basalts from Tallante (eastern Betic Cordillera, southeast Spain) provide an excellent scenario for exploring the metallogenic role of the SCLM beneath a crustal volcanic province hosting a wide range of magmatic-hydrothermal ore deposits. Several studies employed these mantle xenoliths to investigate the multi-stage history of partial melting and metasomatism of the SCLM beneath the western Mediterranean (Beccaluva et al., 2004; Shimizu et al., 2008; Rampone et al., 2010; Bianchini et al., 2011, 2015; Hidas et al., 2016; Marchesi et al., 2017). This well-studied sector of SCLM offers the opportunity to constrain how melting and metasomatism may control the mobility and storage of metals in the mantle. In this study, we integrate a detailed microstructural description of a suite of peridotite xenoliths from Tallante with in situ chemical characterization of their BMS and associated PGM, in order to infer how the metasomatic evolution of the lithospheric mantle may affect the metallogenic fertility of an ore-productive domain of continental crust.

GEOLOGICAL SETTING

The Pliocene alkaline volcanic field of Tallante represents the youngest magmatic episode (2.93–2.29 Ma, Duggen et al., 2005) of the Neogene Volcanic Province (NVP) in southeast Spain (Gómez-Pugnaire et al., 2019, for a review). This province is located in the eastern sector of the Betic Cordillera and consists of a volcanic belt extending NE-SW for ~150 km along the Mediterranean coast (Fig. 1). The NVP comprises Miocene calc-alkaline to ultrapotassic (shoshonitic and lamproitic) volcanic suites. This volcanism changed to alkaline-basaltic activity in the Pliocene-Pleistocene (Duggen et al., 2005). This magmatic evolution, from subduction-related to intraplate magmatism, relates to the complex interplay between compressional shortening along the Iberian-African plate boundary and coeval extensional tectonics in the westward migrating Alborán microcontinent, which eventually collided against the south Iberian and Maghrebian passive margins, thereby generating the arched Betic-Rif Cordillera (e.g., Platt et al., 2013). Stretching of continental lithosphere in response to the westward rollback of the Tethyan subducting slab properly accounts for the regional evolution of the Alborán domain in the Cenozoic (Lonergan and White, 1997). This geodynamic model is supported by geophysical evidence of an east-dipping detached slab beneath the Gibraltar arc (Bezada et al., 2013), and by geochemical signatures of subduction-related fluids/melts in the mantle sources of Miocene tholeiitic and calc-alkaline lavas from the westernmost Mediterranean (Duggen et al., 2004, 2008; Varas-Reus et al., 2017). Westward retreat of the subduction front during the Miocene caused lateral tearing along the continental margin, which was accommodated by subduction transform edge propagator (STEP) faults yielding the topographic uplift of the eastern Betics (Mancilla et al., 2015, 2018). Continental edge delamination of Iberian lithosphere since the late Miocene then marked a shift in the associated magmatism toward high-K calc-alkaline, shoshonitic,

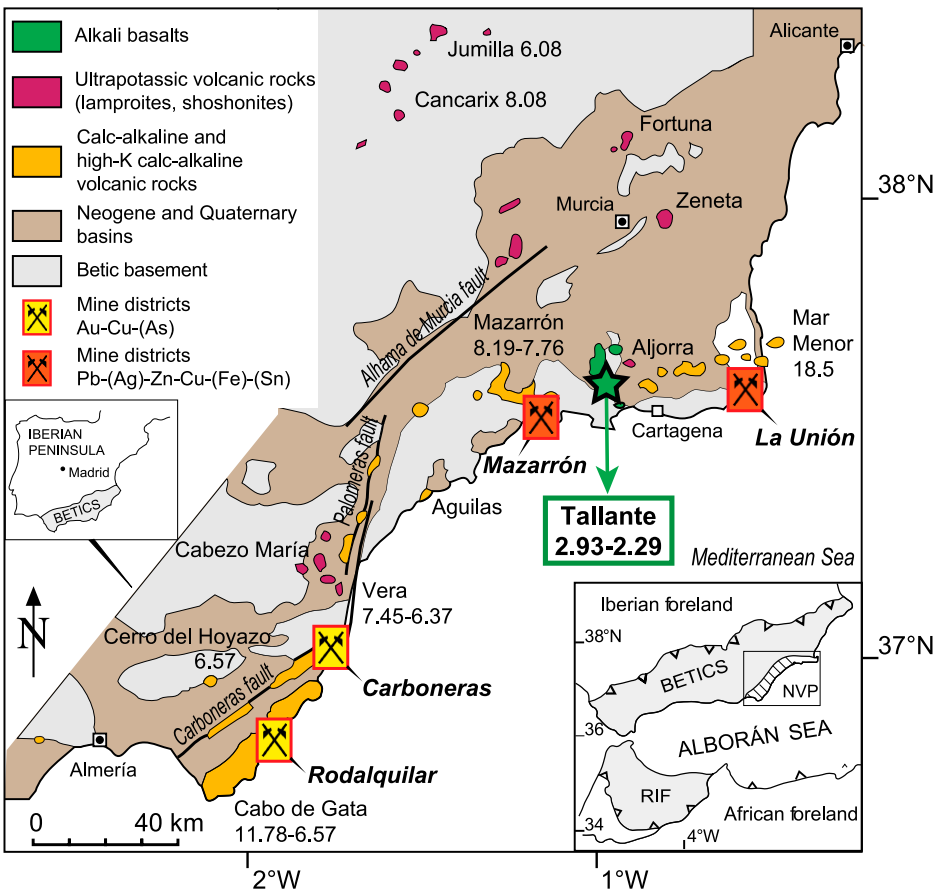

Figure 1. Geological sketch map of the Neogene Volcanic Province (NVP) of southeast Spain with the location of outcrops of different volcanic suites and mining districts (modified from Gómez-Pugnaire et al., 2019). Geochronological data in million years (Ma) of volcanic suites are from Duggen et al. (2008) and references therein.

and lamproitic compositions in response to the asthenosphere upwelling and melting of metasomatized SCLM beneath the southern Iberian margin (Duggen et al., 2005).

Medium- to high-K calc-alkaline volcanism in the NVP (15–6 Ma, Duggen et al., 2008 and references therein) is spatially and genetically associated with important epithermal auriferous (Roadalquilar-Carboneras district) and Pb-Zn-Cu-(Ag) (Mazarrón-La Unión district) ore deposits emplaced in volcanic domes at ca. 11 Ma (Fig. 1) (Arribas et al., 1995; Morales-Ruano et al., 2000; Esteban-Arispe et al., 2016). Hydrothermal fluids, migrating through faults and fractures that acted as magma conduits for the Miocene volcanism (e.g., Carboneras, Palomares, Alhama de Murcia faults) deposited ores in strongly altered calc-alkaline volcanic rocks by mixing of hypersaline magmatic fluids with cooler meteoric solutions (Sänger-von Oepen et al., 1989). Intraplate-type alkaline basalts from Tallante postdate the subduction-related calc-alkaline volcanism associated with ores. Anorogenic signatures of these volcanic rocks reflect a sub-lithospheric mantle source and magma contamination by SCLM components (Duggen et al., 2005). The suite of mantle xenoliths carried by such lavas preserves extreme lithological heterogeneity, which records multiple metasomatic episodes associated with the evolution of the transitional lithosphere underlying the southern Iberian margin (Appendix 1 in the Supplementary Material[1]). Therefore, we expect these mantle peridotites to provide relevant information on the lithospheric mantle reservoir that possibly fed metal endowment in the overlying crust.

SAMPLING AND ANALYTICAL METHODS

In order to identify petrographic domains hosting BMS and PGM in peridotite xenoliths from Tallante, we carried out a careful preliminary examination under a transmitted/reflected light optical microscope in multiple thin sections of 48 xenolith samples. Additional details about the microstructure, geochemistry, and petrology of these xenoliths can be found in Hidas et al. (2016) and Marchesi et al. (2017). Tallante mantle peridotites pervasively record modal metasomatism involving the formation of orthopyroxene and clinopyroxene at the expense of olivine (Rampone et al., 2010; Marchesi et al., 2017). Our petrographic observations document that this main type of silicate metasomatism is closely associated with the presence of BMS, which were detected in clinopyroxene-rich (fertile) lherzolites. Therefore, 14 thin sections from six different samples of these rocks were selected to investigate for the first time the mineral repositories of noble metals and semi-metals in the Tallante peridotite xenoliths. The methodological approach of this study was based on the coupling of detailed microstructural observations on thin sections using field emission gun–environmental scanning electron microscopy (FEG-ESEM) with in situ chemical characterization of major and trace elements using electron microprobe analyzer (EMPA) and laser ablation–inductively coupled plasma–mass spectrometry (LA-ICP-MS) in both silicate and sulfide minerals. Detailed description of the analytical methods performed in this study is presented in Appendix 2 of the Supplementary Material (see footnote 1).

PETROGRAPHY AND MINERAL CHEMISTRY OF SULFIDE-BEARING PERIDOTITES

All the sulfide-bearing mantle xenoliths from Tallante selected for this study are spinel lherzolites (see fig. S1 in Marchesi et al., 2017), which mainly consist of medium- to fine-grained (0.5–2 mm) olivine, orthopyroxene, clinopyroxene, and spinel (Figs. 2A–2D). Interstitial films and/or patches of glass are common around clinopyroxene and spinel grains (Figs. 2E and 2F). Plagioclase is present only in one sample (TAL128), both as rims around spinel and interstitial anhedral patches. Accessory amphibole (pargasite) is locally included in clinopyroxene. Base-metal sulfides always constitute inclusions hosted in clinopyroxene and, to a lesser extent, orthopyroxene (Figs. 2D–2F).

Silicates and Spinel

Slightly strained, polygonal olivine grains generally have granoblastic to equigranular texture, which likely formed during pervasive melt percolation at the expense of former porphyroclastic microstructure (Rampone et al., 2010). Few relics of olivine porphyroclasts show kink bands, subgrain boundaries, and shape-preferred orientation—marking a weak foliation—indicative of crystal-plastic deformation prior to the equigranular recrystallization. On the other hand, orthopyroxene and clinopyroxene usually form amoeboid, unstrained crystals or irregular patches interstitially scattered between olivine (Figs. 2A–2D). Orthopyroxene also forms tabular to anhedral crystals that seem to replace olivine, as suggested by lobate rims and poikilitic textures (Figs. 2A and 2C). Closely-spaced cleavage planes and exsolution lamellae are locally observed within both types of pyroxene (Figs. 2A and 2B). Dark brown spinel forms subspherical blebs or amoeboid grains interstitial between olivine, locally iso-oriented into linear trails sub-parallel to the sample foliation (Rampone et al., 2010). Moreover, anhedral spinel is commonly in close contact with sulfide-hosting clino- and orthopyroxene forming mineral intergrowths (Figs. 2A, 2C, and 2D) that are scattered between matrix olivine, uncontrolled by the macroscopic foliation and without penetrative shape preferred orientation. In places, these sulfide-bearing clinopyroxene-orthopyroxene-spinel intergrowths have straight internal contacts (Figs. 2A and 2D), whereas both types of pyroxene and spinel display curvilinear grain boundaries and cusp-shaped terminations against olivine (Fig. 2A–2D).

Olivine in the matrix has Mg# [$100 \times Mg/(Mg + Fe^{2+})$] from 88.8 to 91.1 and CaO contents below the EMPA detection limit (Fig. 3A). Orthopyroxene has Mg# ranging from 89.6 to 91.8, and its Al_2O_3 contents (2.46–5.66 wt%) are positively correlated with Cr_2O_3 (0.22–1.05 wt%) and TiO_2 (0.01–0.47 wt%), and negatively with SiO_2 (53.2–56.8 wt%). Clinopyroxene shows a preferential distribution pattern defined by decreasing Al_2O_3, Cr_2O_3, and TiO_2 (Figs. 3B and 3C), and increasing Mg# (89.8–93.6) and SiO_2 (49.1–53.7 wt%) (not shown) from core to rim. These variations have been interpreted to reflect re-equilibration of clinopyroxene during mantle decompression and cooling (Hidas et al., 2016). Clinopyroxene grains in the plagioclase-bearing lherzolite (TAL128) have TiO_2 abundances that are significantly higher than those in plagioclase-free samples, coupled with relatively low Cr_2O_3 and high Al_2O_3 contents (Figs. 3B and 3C). Similar compositional trends were described in clinopyroxene from plagioclase-bearing peridotites impregnated by exotic melts (Rampone et al., 1997). Amoeboid spinel between olivine or associated with pyroxenes has Mg# = 74.5–81.6, Cr# [Cr/(Cr + Al)] = 0.11–0.27, and low TiO_2 abundances (<0.15 wt%) (Table S1; see footnote 1), which are slightly higher in the plagioclase-bearing sample (Fig. 3D).

[1]Supplemental Material. Appendix 1: Petrogenesis of Tallante mantle xenoliths; Appendix 2: Analytical methods; Table S1: Major element compositions of rock-forming minerals in Tallante xenoliths; Table S2: Major element compositions of base-metal sulfides (in wt%); Table S3: trace elements abundances (ppm) of clinopyroxene grains in Tallante xenoliths; Table S4: concentrations (ppm) of chalcophile and siderophile elements in base-metal sulfides. Please visit https://doi.org/10.1130/GSAB.S.15911937 to access the supplemental material, and contact editing@geosociety.org with any questions.

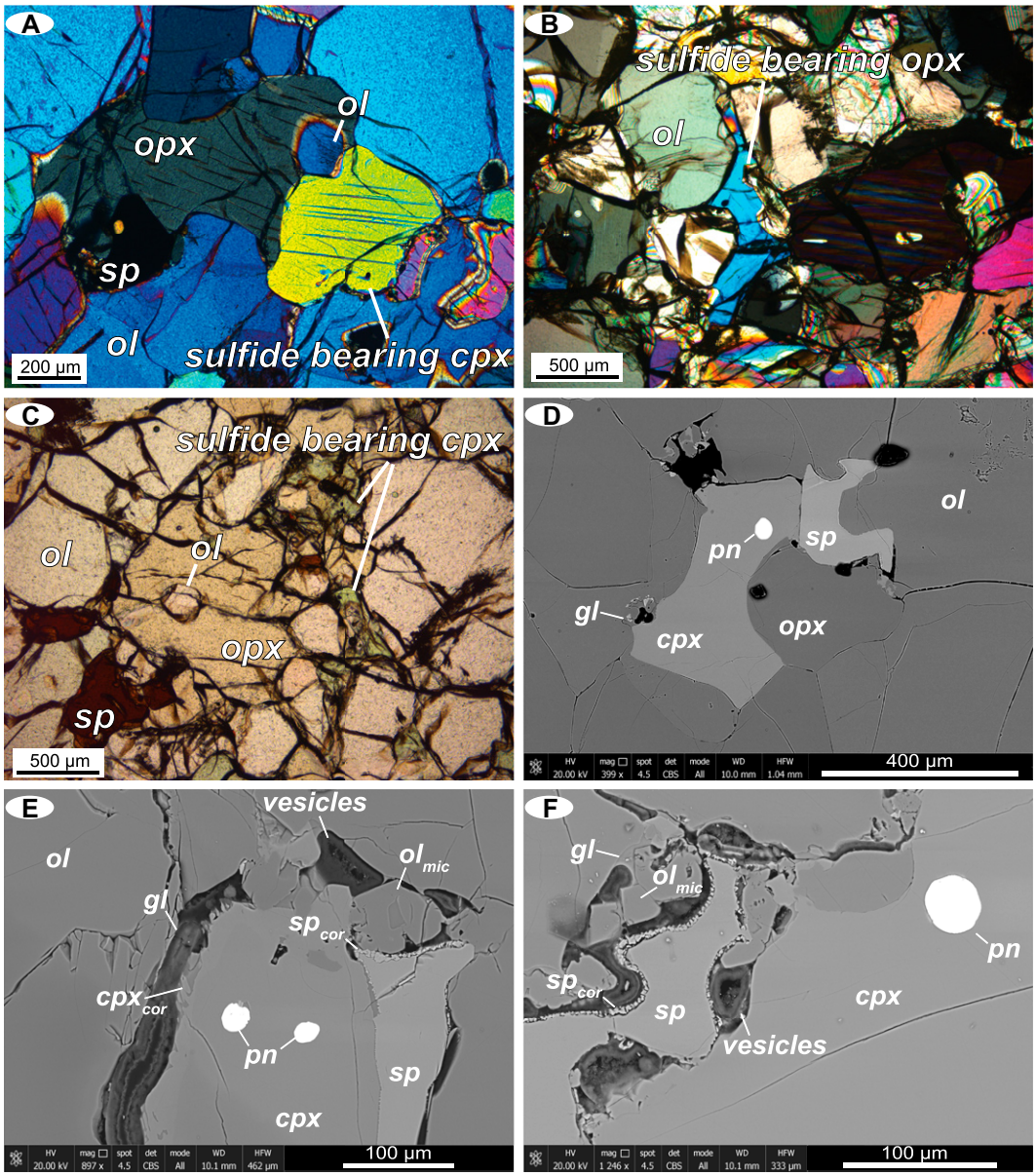

Figure 2. Photomicrographs of polarized light optical microscope (A, B, C) and backscattered electron images (D, E, F) of sulfide-bearing domains in spinel lherzolites from Tallante, southeast Spain. Mineral abbreviations are: ol—olivine; cpx—clinopyroxene; opx—orthopyroxene; sp—spinel; gl—glass; cpx_{cor}—spongy coronae of clinopyroxene; sp_{cor}—spongy coronae of spinel; ol_{mic}—olivine microlites; pn—pentlandite.

Interstitial Glass Pockets

Glass forms lobate pockets and interstitial patches with irregular contacts against clinopyroxene and spinel grains (Figs. 2E and 2F). These pockets consist of a matrix of silicate glass, small (<50 µm) euhedral crystals (microlites) of olivine and spinel, and abundant subspherical vugs and vermicular vesicles (Figs. 2E and 2F). Coarse spinel and clinopyroxene in contact with interstitial glass usually exhibit secondary rims made of spongy coronae and porous overgrowths (Figs. 2E and 2F).

Interstitial glass has silica-rich (54.6–61.2 wt%) major element compositions, also enriched in Al_2O_3 (19.7–23.2 wt%) and Na_2O (2.14–5.92 wt%), and depleted in MgO (1.34–3.59 wt%), FeO (1.70–2.95 wt%), and K_2O (<0.03 wt%), and present variably low total oxides (Table S1). Both euhedral microlites and coronitic overgrowths in contact with glass pockets have major element compositions that clearly differ from those of the grain cores and coarse grains in the matrix (Fig. 3). Olivine microlites have higher Mg# (90.0–92.5) and CaO contents (0.10–0.31 wt%) than matrix olivine (Fig. 3A), and spinel microlites are enriched in TiO_2 (0.35–0.49 wt%) compared with coarse spinel (Fig. 3D). On the other hand, clinopyroxene in spongy coronae is usually enriched in Al_2O_3 (5.76–8.75 wt%), Cr_2O_3 (1.09–2.88 wt%), and TiO_2 (0.81–1.65 wt%) compared with inner portions of the grains (Figs. 3B and 3C). The spongy coronae of spinel have higher Cr# (0.35–0.38) and TiO_2 (0.33–0.36 wt%) compared with the grain core (Fig. 3B).

Base-Metal Sulfides

Base-metal sulfides are droplet-like inclusions (10–50 µm) always hosted in anhedral clinopyroxene and orthopyroxene (Figs. 2D–2F), without any textural relationship with internal fractures or cracks of the host pyroxene. They are monomineralic or polyphase aggregates consisting of pentlandite locally coexisting with chalcopyrite and/or bornite grains (Figs. 4A–4C). Chalcopyrite also forms spatially arranged planar intergrowths within larger pentlandite grains (Fig. 4D). Locally, grains of pentlandite and bornite are rimmed either by millerite or chalcocite (Fig. 4B).

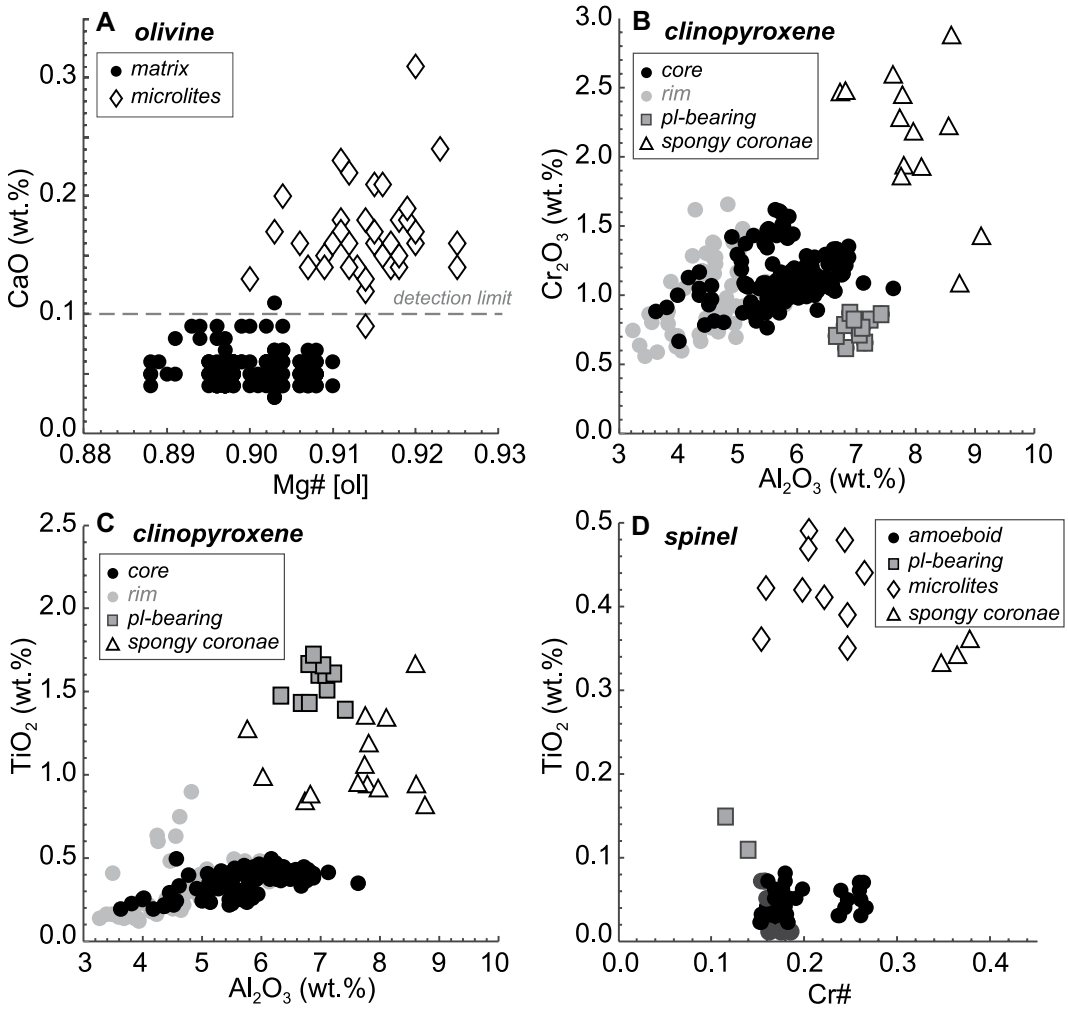

Figure 3. Mg# [100 × Mg/(Mg + Fe^{2+})] versus CaO (wt%) in olivine (A), Al_2O_3 versus Cr_2O_3 (B) and TiO_2 (wt%) (C) in clinopyroxene, and Cr# [Cr/(Cr + Al)] versus TiO_2 (wt%) in spinel (D) in peridotite xenoliths from Tallante (southeast Spain). Black and gray circles indicate the compositions of cores and rims of grains in the matrix, respectively; white diamonds and triangles mark the compositions of microlites and spongy coronae, respectively; gray squares represent the compositions of minerals in the plagioclase (pl)-bearing lherzolite samples (TAL128).

Pentlandite has metal/S atomic ratios ranging from 1.10 to 1.13, and Ni/(Ni + Fe) atomic ratios from 0.56 to 0.68 (Fig. 5A). Cobalt and Cu contents are generally below 0.32 wt% and 0.90 wt%, respectively (Table S2 in the Supplementary material; see footnote 1). However, Cu contents up to 4.37 wt% are detected in pentlandite grains with abundant chalcopyrite intergrowths (cf. *mixed analyses Table S2). Chalcopyrite coexisting with pentlandite in composite aggregates has metal/S ratio ~1 (Fig. 5B) and Ni contents up to ~5 wt% probably due to analytical interference with adjacent pentlandite. Bornite spans from Fe-enriched (Fe = 13.7 wt%) to sulfur-deficient, Cu-enriched compositions (Cu = 68.9 wt%) approaching that of chalcocite (Fig. 5B). The retrieved bulk compositions of polyphase aggregates have metal/S atomic ratios ranging from 1.07 to 1.14, Ni/(Ni + Fe) = 0.51–0.59, which is slightly lower than in monomineralic pentlandite, and high Cu contents ranging from 6.24 to 14.8 wt% (Table S2 in the Supplementary Material).

Some BMS in the Tallante peridotite xenoliths contain nano-to-micrometer sized PGM. These grains consist of euhedral inclusions, usually less than 1 to ~5 μm in size, which commonly occur close to the grain boundary between sulfide and pyroxene (Fig. 6A) without any connection to internal fractures or cracks (Fig. 6B). Qualitative identification by EDS microanalyses indicates that these PGM usually consist of Pt(-Pd)-Sn (Figs. 6A and 6B). The focused ion beam and transmission electron microscopy (TEM) analysis carried out by González-Jiménez et al. (2020) revealed that these PGM are crystals of tatyanite (ideally $Pt_9Cu_3Sn_4$) with no crystallographic continuity with host pentlandite. Furthermore, we detected several nanometer-sized grains of native gold (±platinum) included in pentlandite grains. Gold particles display well defined crystal shapes and needle-like morphologies (Fig. 6C). Again, there is no textural feature, such as fractures or cracks, controlling the location of the gold particles in the host sulfide. A more precise qualitative identification by EDS microanalyses of these grains is partially hindered by the matrix interferences of major elements (S, Fe, Ni, Cu) in the host sulfide.

TRACE ELEMENT COMPOSITIONS

Sulfide-Hosting Clinopyroxene

Coarse clinopyroxene displays rare earth element (REE) concentrations from ~3–40 times the chondritic values (McDonough and Sun, 1995), with concentrations of most samples between 4 and 10 times chondritic (Figs. 7A and 7B). Clinopyroxene grains in plagioclase-free spinel lherzolites are, in general, light REE (LREE)-depleted (La_N/Sm_N = 0.35–0.85), and present variable middle REE (MREE) over heavy REE (HREE) fractionation (Sm_N/Yb_N = 0.68–1.25) and rather homogeneous HREE contents (Yb_N = 6–11; Fig. 7A). These data are consistent with previous results of clinopyroxene in spinel lherzolites from Tallante (Beccaluva et al., 2004; Rampone et al., 2010; Bianchini et al., 2011; Marchesi et al., 2017). However, clinopyroxene from different samples has slightly different REE distributions (Fig. 7A). Analyzed grains in TAL110, TAL129, TAL143, and TAL146 exhibit rectilinear enrichment from

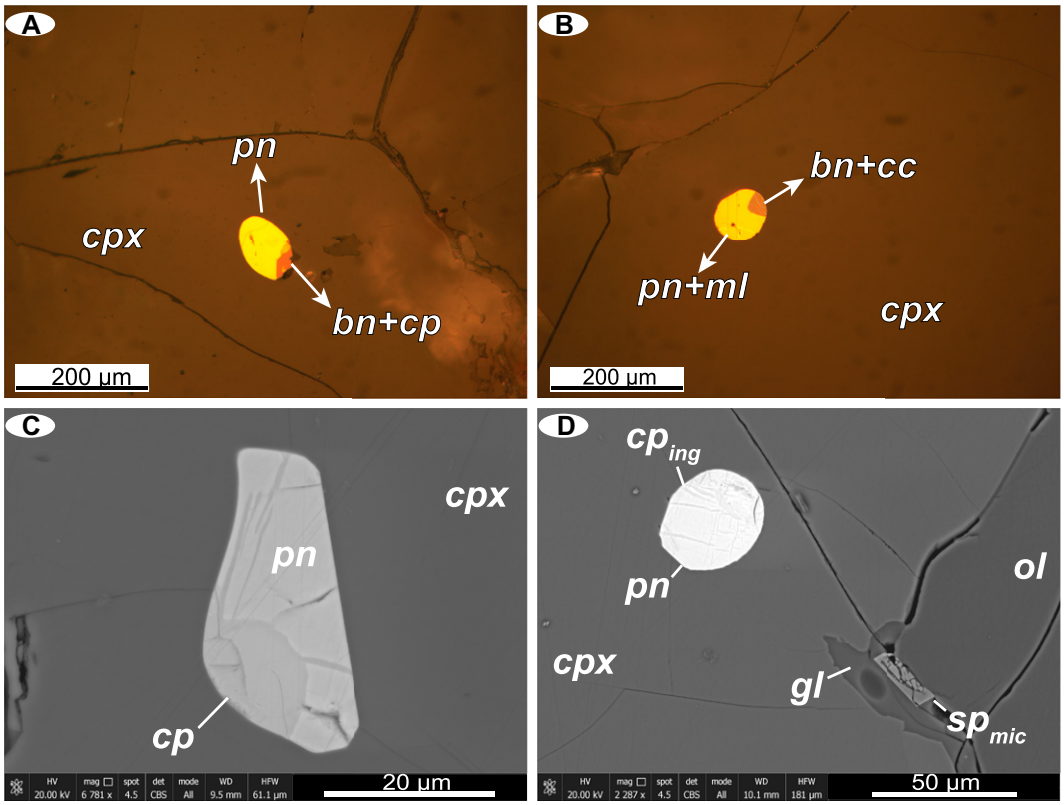

Figure 4. Photomicrographs of base-metal sulfide assemblages in Tallante (southeast Spain) peridotite xenoliths: reflected light optical (A, B) and BSE images (C, D). Mineral abbreviations as in Figure 2, and cp—chalcopyrite (ing—intergrowths); bn—bornite; cc—chalcocite; sp_{mic}—spinel microlites.

LREE to MREE (La_N/Sm_N = 0.35–0.85) (type 1a), while grains in sample TAL099 generally have more fractionated LREE-MREE segments (La_N/Sm_N = 0.39–0.49) (type 1b). Furthermore, a few clinopyroxene grains from TAL110 and TAL129 are enriched in LREE relative to MREE (La_N/Sm_N = 1.46–3.06) (type 1c). Clinopyroxene from plagioclase-bearing lherzolite (sample TAL128) displays convex-upward MREE-enriched patterns (La_N/Sm_N = 0.32–0.40; Sm_N/Yb_N = 1.81–2.02) (type 2), analogous to previous observations in clinopyroxene from plagioclase-bearing lherzolites from Tallante (Rampone et al., 2010). Finally, spongy coronae of clinopyroxene in contact with interstitial glass are in general more depleted in LREE (especially La and Ce) than coarser clinopyroxene from the matrix, whereas MREE and HREE have similar concentrations (Fig. 7A).

Heterogeneous LREE/MREE patterns are coupled with different concentrations of other incompatible trace elements (Figs. 7C and 7D). Clinopyroxene in plagioclase-free spinel lherzolites displays chondrite-normalized multi-element diagrams (Fig. 7C) characterized by variable negative anomalies of high-field strength elements (Nb, Ta, Zr, Hf, Ti) relative to adjacent REE of similar compatibility, coupled with Th-U positive spikes. However, the extent of Th-U enrichment is linked to LREE/MREE fractionation. Thus, LREE-enriched clinopyroxene (type 1c) has higher concentrations of Th-U relative to Nb-Ta (Th_N/Nb_N = 10.3–98.6),

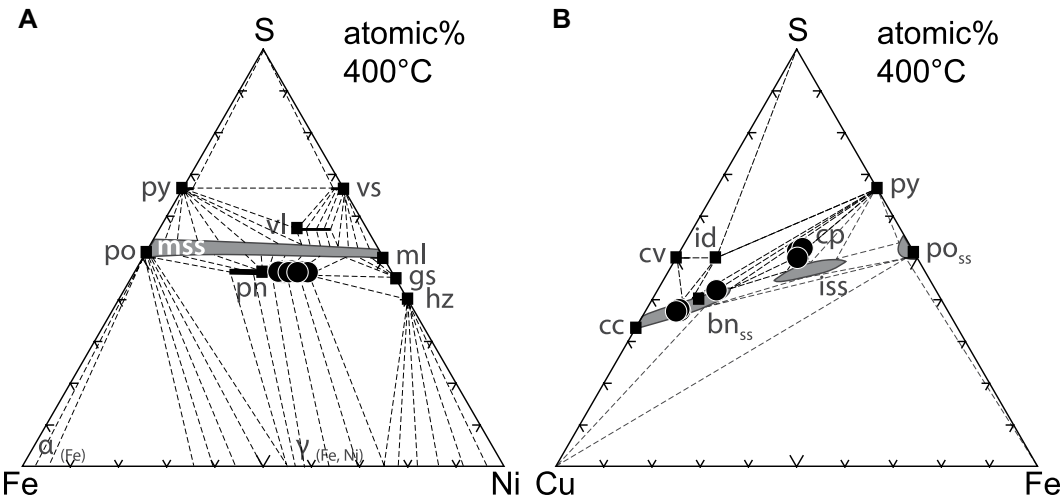

Figure 5. Major element compositions (atomic%) of base-metal sulfides in Tallante (southeast Spain) peridotites (black circles) plotted in the Fe-Ni-S (A) and Cu-Fe-S (B) phase diagrams. Phase relations at 400 °C are from Kullerud et al. (1969) for the Fe-Ni-S system, and Cabri (1973) for the Cu-Fe-S system. Mineral abbreviations: pn—pentlandite; po—pyrrhotite; mss—monosulfide solid solution; ml—millerite; hz—heazlewoodite; py—pyrite; vs—vaesite; vl—violarite; gs—godlevskite; bn—bornite solid solution; iss—intermediate solid solution; cv—covellite; cc—chalcocite; cp—chalcopyrite; id—idaite.

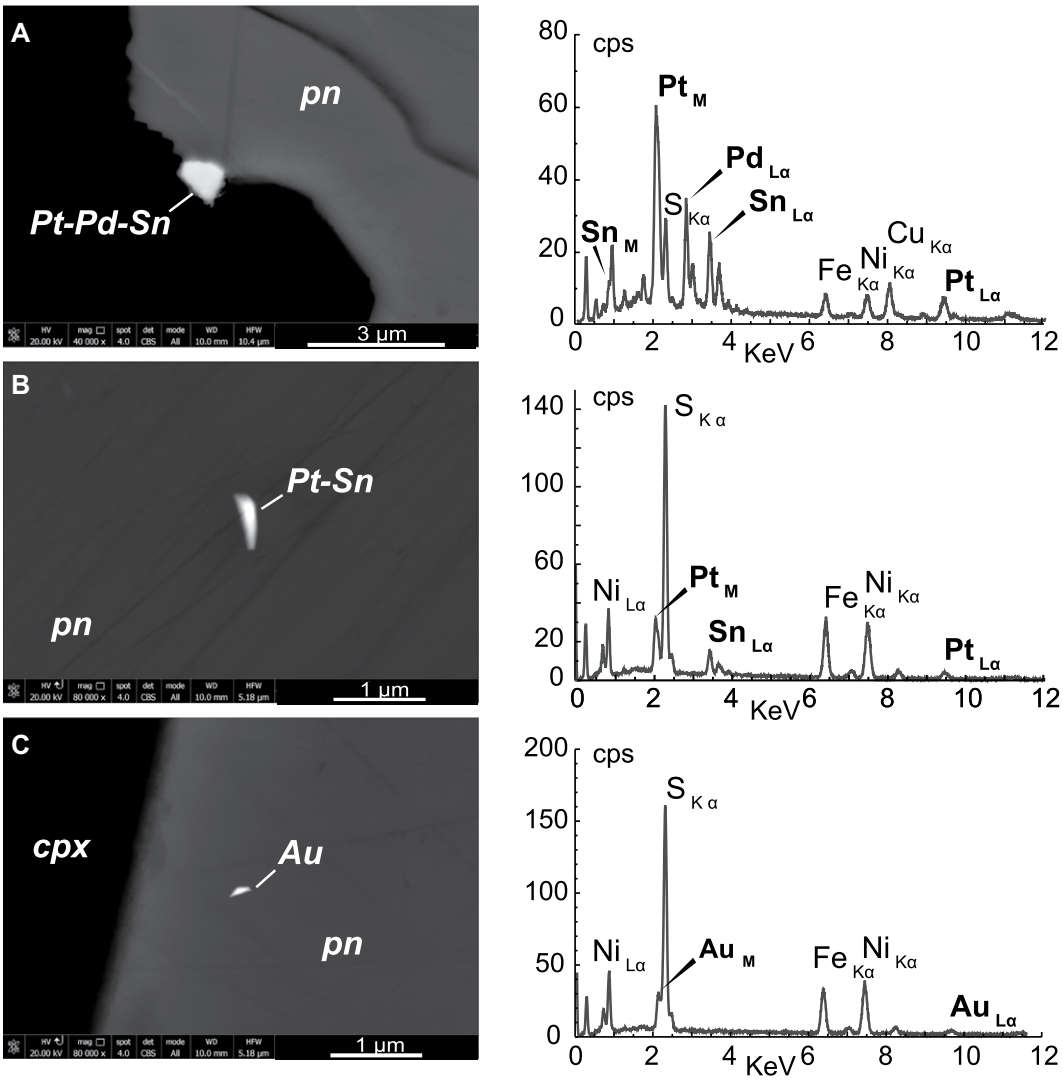

Figure 6. Backscattered electron images and corresponding energy-dispersive X-ray spectroscopy spectra of sulfide-hosted tatyanite ($Pt_9Cu_3Sn_4$) (A), Pt-Sn rich platinum-group mineral (PGM) (B), and native gold (C) in peridotite xenoliths from Tallante (southeast Spain). S-Ni-Fe-Cu peaks in EDS spectra in part are due to contamination by the host sulfide. pn—pentlandite; cps—counts per second; cpx—clinopyroxene.

whereas clinopyroxene with lower LREE/MREE ratios (type 1b) has a weaker positive Th-U anomaly ($Th_N/Nb_N = 1.08–11.7$) and lower Nb_N/Ta_N ratio (0.16–0.52). The less fractionated LREE/MREE type 1a clinopyroxene exhibits transitional features between these two signatures ($Th_N/Nb_N = 1.61–56.9$). Grains with stronger enrichment of Th-U (type 1c) are also more depleted in Ti and Zr relative to adjacent REEs. Lead (Pb) is notably poor in all types of grains (Fig. 7C). Clinopyroxene in plagioclase-bearing peridotites (TAL128: type 2) displays low Th-U enrichment ($Th_N/Nb_N = 1.18–7.74$) coupled with strong subchondritic Nb_N/Ta_N (0.04–0.15) (Fig. 7D). Moreover, these grains also have higher Zr-Ti and lower Sr contents compared with clinopyroxene in plagioclase-free lherzolites. Similar clinopyroxene patterns in other plagioclase-impregnated peridotites from Tallante have been ascribed to melt-rock reaction at decreasing melt mass and/or entrapment of small fractions of melt (Rampone et al., 2010).

Base-Metal Sulfides

In situ chalcophile and siderophile elements data were obtained for BMS inclusions in pyroxene consisting of monomineralic pentlandite (e.g., Figs. 2E and 2F), pentlandite with chalcopyrite intergrowths (e.g., Fig. 4D), and pentlandite coexisting with chalcopyrite and/or bornite grains (e.g., Figs. 4A and 4C). The concentrations of PGE and Au in the analyzed BMS (n = 67) are variable and range from 0.470 to 75.3 ppm for Os, 0.370–44.0 ppm for Ir, 1.08–79.9 ppm for Ru, 0.442–14.4 ppm for Rh, 0.194–383 ppm for Pt, 0.970–247 ppm for Pd, and 0.104–46.3 ppm for Au (Table S4 in the Supplementary Material; see footnote 1). The time-resolved spectra of I-PGE (Os, Ir, Ru) and Rh show constant count rates with respect to Ni as a function of ablation time, suggesting that these elements are structurally bound in the BMS. In contrast, the signals of Pt, Au, and in some cases Pd show sharp peaks in the time-resolved spectra of several sulfides, revealing the presence of discrete Pt-, Au-, and Pt-Pd-Au-bearing micro-inclusions dispersed within the host BMS (Fig. 8). These submicrometer-sized nuggets, which were already observed as crystal phases during scanning electron microscope (SEM) analyses (Fig. 6), are thought to be the reason for the high contents of Pt, Au, and sometimes Pd in several analyzed BMS, whereas low concentrations of these elements are generally associated with the lack of positive spikes in the time-resolved spectra.

Three distinct groups of chondrite-normalized PGE patterns (normalizing values from Fischer-Gödde et al., 2010) were identified based on their Pd_N/Ir_N ratios in the whole suite

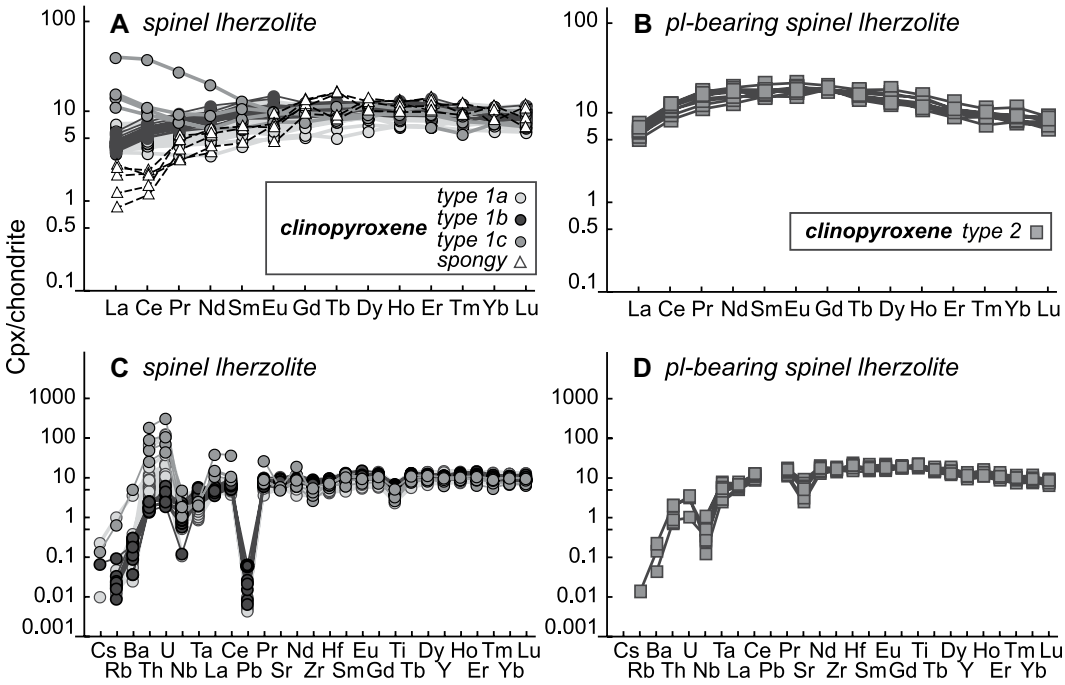

Figure 7. Chondrite-normalized concentrations of rare earth elements and other lithophile trace elements in clinopyroxene (Cpx) of spinel lherzolites (A, C) and plagioclase-bearing lherzolite (B, D) from Tallante, southeast Spain. Light gray, black, and dark gray circles in (A) and (C) indicate the compositions of grains with different La_N/Sm_N fractionations (types 1a, 1b, 1c), and white triangles the compositions of spongy coronae of clinopyroxene in spinel lherzolites; pl—plagioclase. Normalizing values from McDonough and Sun (1995).

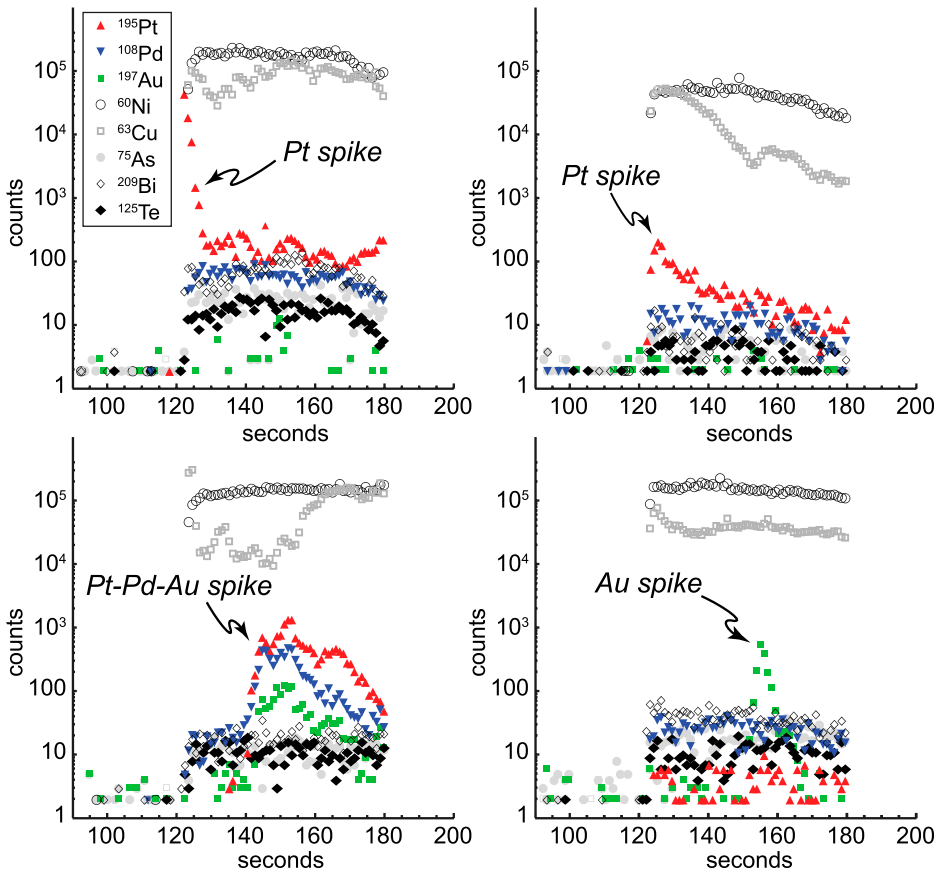

Figure 8. Representative time-resolved spectra of laser ablation–inductively coupled plasma–mass spectrometry analyses for selected isotopes in base-metal sulfides of Tallante peridotites, southeast Spain.

of BMS (Fig. 9), regardless of the assemblage constituting the analyzed inclusion: (1) nearly flat PGE patterns with variable enrichment in P-PGE (Pd_N/Ir_N = 1.03–4.56) (n = 37; Fig. 9A), (2) arch-shaped PGE patterns with an almost flat segment from Os to Rh and a negatively fractionated segment from Rh to Pd (Pd_N/Ir_N = 0.14–0.90) (n = 19; Fig. 9B), and (3) positively fractionated PGE patterns with low I-PGE contents and suprachondritic Pd_N/Ir_N ratios (5.28–30.74) (n = 11; Fig. 9C). Interestingly, the analyzed BMS may display depletion in Pt and Au down to less than 0.5 times the chondritic concentrations, regardless of the compositional group (Pd_N/Ir_N ratio) to which they belong (Figs. 9A–9C). A careful inspection of their respective time-resolved spectra reveals that negative anomalies are detected when Au- or Pt-spikes (Fig. 8) are lacking.

Abundances of semi-metals vary from 91.3 to 225 ppm for Se, 5.36–116 ppm for As, 10.3–42.6 ppm for Te, 0.274–3.02 ppm for Sb, and 0.350–9.79 ppm for Bi (Table S4 in the Supplementary Material). Their signals in the time-resolved spectra are homogeneous with respect to Ni, suggesting they entered in solid solution in the BMS (Fig. 8). The normalized concentrations of these elements ordered from left to right according to their atomic radius are similar for the three sulfide groups with different Pd_N/Ir_N fractionations (Figs. 9D–9F). Noteworthy, Te and, especially, Bi are slightly

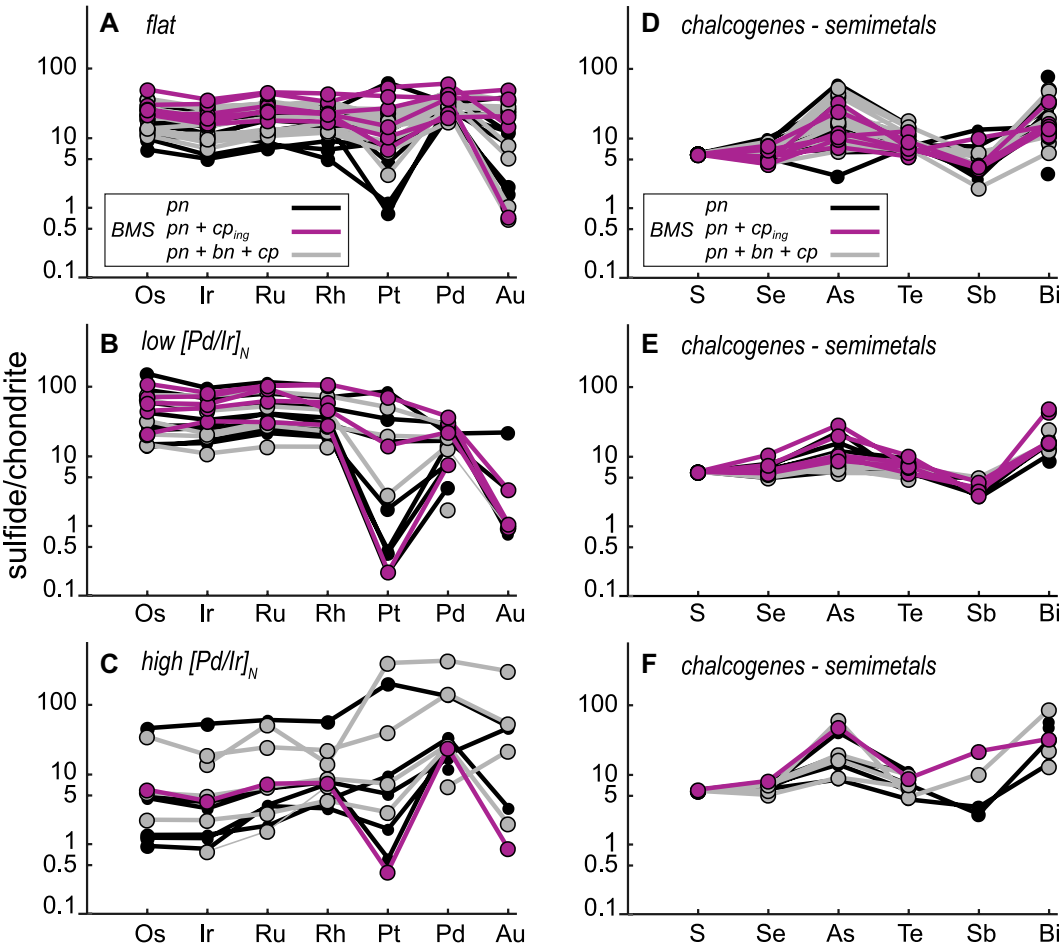

Figure 9. Chondrite-normalized abundances of platinum-group elements (PGE) (A, B, C) and semi-metals (D, E, F) in base-metal sulfides (BMS) with different Pd_N/Ir_N fractionations from Tallante peridotites, southeast Spain. Both PGE and semi-metals are ordered from left to right according to decreasing compatibility in monosulfide solid solution coexisting with a sulfide liquid. Black lines indicate patterns of monomineralic pentlandite (pn), purple lines of pentlandite + chalcopyrite intergrowths (cp_{ing}), and gray lines of pentlandite + bornite + chalcopyrite (pn + bn + cp). Normalizing values are from Fischer-Gödde et al. (2010) and McDonough and Sun (1995).

enriched in all grains, whereas As has variable abundances defining significant positive anomalies (Figs. 9D–9F). The extent of the positive As anomaly does not show any correlation with either Pd_N/Ir_N fractionation or with depletion in Pt and Au.

DISCUSSION

Metasomatic Origin of Sulfide-Hosting Clinopyroxene

The granoblastic texture of the sulfide-bearing peridotite xenoliths from Tallante records annealing recrystallization of the olivine fabric in response to pervasive percolation of silicate melts (Rampone et al., 2010; Hidas et al., 2016). Sulfide-hosting anhedral pyroxenes are commonly associated with spinel, forming irregular intergrowths scattered between olivine grains (Fig. 2). The distribution of these clinopyroxene + orthopyroxene + spinel intergrowths lacks any geometric control by the olivine fabric, suggesting they formed subsequently to the deformational stage that produced the sample foliation. Moreover, both pyroxenes and spinel frequently corrode or include olivine through lobate rims or poikilitic texture (Figs. 2A–2D), supporting that they formed by melt-rock interaction rather than by garnet breakdown as proposed by Shimizu et al. (2008) and Rampone et al. (2010). This interpretation is consistent with modal metasomatism causing FeO-SiO_2 enrichment in these fertile spinel lherzolites (Marchesi et al., 2017). Reactive percolation of silicate melts by porous flow in peridotite xenoliths from Tallante is further documented by crystallization of olivine rims replacing orthopyroxene, or vice versa (Rampone et al., 2010). Sulfide droplets are systematically included within metasomatic clino- and orthopyroxene (Figs. 2D–2F and 4), suggesting that their precipitation took place when the percolating silicate melt shifted from olivine- to pyroxene-saturation while rising adiabatically and interacting with host peridotites (Rampone et al., 2010).

Variations in the abundances of trace elements in clinopyroxene (Fig. 7) likely reflect their chromatographic fractionation during interaction of lithospheric mantle with percolating melt (Navon and Stolper, 1987). As chemical exchange between melt and peridotite wall-rock is faster for the more incompatible elements, comparatively stronger compositional heterogeneities are expected for large ion lithophile elements (LILE: Cs, Rb, Ba), LREE, and high-field strength elements (HFSE: Nb, Ta, Th, and U). Therefore, the progressive shift from LREE-depleted (types 1a and 1b) to LREE-enriched patterns (type 1c) of sulfide-hosting clinopyroxene (Fig. 7A) was probably produced by the reaction with silicate melts at decreasing melt/rock ratios (Bedini et al., 1997; Ionov et al., 2002). The stronger positive U-Th peaks coupled with higher LREE concentrations and Nb_N/Ta_N ratios observed in a few clinopyroxene grains (type 1c, Fig. 7C) are possibly due to late-stage interaction with small melt fractions, which finally evolved toward compositions more enriched in incompatible elements as a consequence of their progressive differentiation and percolation through the SCLM (Bedini et al., 1997; Rampone et al., 2010).

The age of norite veins cross-cutting peridotites in composite mantle xenoliths from Tallante (6.8 ± 2.0 Ma) (Bianchini et al., 2015) indicates that the metasomatic event producing the formation of sulfide-hosting pyroxene predated the late Miocene–Pleistocene alkaline magmatic cycle

in the eastern Betic Cordillera (Duggen et al., 2005). According to Bianchini et al. (2011), Sr-Nd-Hf isotopes of clinopyroxene corroborate that Jurassic MORB-type silicate melts were the main metasomatic agent in the Tallante lithospheric mantle. However, the lack of geochemical equilibrium between different clinopyroxene grains at the thin section scale (Fig. 7) argues against an old Mesozoic percolation event in these rocks. Indeed, the general LREE-depleted signature of clinopyroxene in extensively percolated peridotites from Tallante has been ascribed to pervasive re-equilibration with Cenozoic tholeiites of subduction-related affinity (Rampone et al., 2010). Based on the wide variability of Sr-Nd-Pb isotopic signatures, Marchesi et al. (2017) ascribed the microstructural and compositional features of metasomatic clinopyroxene to reactive porous flow of melts from a pyroxenite-bearing heterogeneous mantle source.

Melts with a pyroxenite component played a key role in the geochemical refertilization of the SCLM beneath the western Mediterranean (Lambart et al., 2012; Marchesi et al., 2014). Thermodynamic and experimental work indicates that clinopyroxene, orthopyroxene, and spinel crystallize from a pyroxenite-derived melt interacting with peridotite (Lambart et al., 2012). Depending on the silica activity of this melt, either olivine or orthopyroxene occurs on the liquidus surface together with clinopyroxene ± spinel (Lambart et al., 2012), properly accounting for the coupled dissolution of olivine and formation of orthopyroxene, or vice versa, recorded by the whole set of Tallante spinel peridotites (Rampone et al., 2010; Marchesi et al., 2017). In the context of the geodynamic evolution of the western Mediterranean, partial melting of a pyroxenite-peridotite veined mantle was likely caused by lithospheric extension and asthenosphere upwelling due to westward rollback retreat of the subduction system in the Cenozoic (Duggen et al., 2005, 2008). In summary, previous works and our new compositional and textural observations support the hypothesis that the metasomatic event leading to crystallization of sulfide-hosting pyroxene was due to the Miocene subduction-related subalkaline metasomatism permeating the southern Iberian lithosphere in response to the upwelling of a hot asthenospheric mantle upon slab rollback and tearing of the continental paleomargin (Mancilla et al., 2015; Hidas et al., 2016).

In Situ Melting of Metasomatic Domains

Interstitial glass within Tallante spinel lherzolites forms vug-rich lobate pockets that border clinopyroxene and spinel (Figs. 2E and 2F). The absence of glass around domains constituted by olivine, the main rock-forming mineral, rules out the hypothesis that it represents external melt infiltrating the peridotites. In addition, glass pockets are remarkably enriched in SiO_2 and Al_2O_3 (Fig. 10), and depleted in MgO, FeO, TiO_2, and K_2O (not shown) compared with host alkali basalts (Fig. 10), supporting the idea that they are not simply portions of host magma trapped in the xenoliths (Coltorti et al., 2000; González-Jiménez et al., 2014; Tassara et al., 2018). Homogeneous TiO_2/Al_2O_3 ratios (~0.04–0.07) over the whole range of SiO_2 abundances in glass (Fig. 10) are also inconsistent with reaction between peridotite and infiltrating alkali basaltic melts (Neumann and Wulff-Pedersen, 1997). Moreover, amphibole and phlogopite relics are absent in the matrix of the studied spinel lherzolites, arguing against an origin of glass by incongruent breakdown of these phases (Yaxley et al., 1997).

On the other hand, the exclusive association of glass with metasomatic clinopyroxene-spinel assemblages supports its generation by in situ melting of small-scale mineral domains formed during Miocene refertilization. Indeed, the compositions of glass (Table S1) resemble those of near-solidus melts of fertile spinel peridotites at low pressure (1 GPa) (Fig. 10) (Baker et al., 1995; Falloon et al., 2008). Empty vugs and subspherical vesicles in glass pockets (Figs. 2E and 2F) suggest that a significant amount of volatiles were originally dissolved in the melt now quenched to silicate glass. This supports that melting occurred under hydrous conditions, possibly explaining the SiO_2-rich composition of several interstitial glass patches compared with anhydrous near-solidus melts (Fig. 10) (Gaetani and Grove, 1998). In this scenario, volatiles likely lowered the solidus temperature of spinel lherzolites at low pressure, promoting the small-scale melting of sulfide-hosting clinopyroxene and spinel (Ionov et al., 1994). This local event should have occurred at very low melting degrees, thus preserving most of the clinopyroxene-spinel assemblages and generating small amounts of melts, which were unable to segregate through interconnected channels (von Bargen and Waff, 1986) and were instead trapped at interstices in close contact with their source minerals. The irregularly shaped geometries of glass patches (Figs. 2E and 2F) contrast with the equilibrium melt distribution predicted for a partially molten peridotite at mantle conditions (Jin et al., 1994), suggesting that the entrapment of melt pockets occurred in a relatively short time.

At contacts with glass, clinopyroxene, and spinel usually display spongy coronae (Figs. 2E and 2F) that constitute a reaction zone with quenched melt ("spongy textures" in Kovács et al., 2007; Pan et al., 2018). This melt-mineral reaction led to higher contents of Al_2O_3, TiO_2, and Cr_2O_3 in spongy clinopyroxene, as well as of TiO_2 in spongy spinel, in comparison with the inner portion of the grains (Figs. 3B–3D). In addition, enhanced partitioning of Ti in clinopyroxene at near-solidus melting conditions (Baker et al., 1995) may have contributed to enrich TiO_2 in spongy clinopyroxene. Low degrees of partial melting at grain rims may explain lower LREE concentrations in spongy clinopyroxene (Fig. 7A) and slightly higher Cr# in spongy spinel (Fig. 3B) (Yaxley et al., 1997; Kovács et al., 2007). However, higher Cr# in spinel may also reflect low-pressure re-equilibration of spongy coronae with Si-rich hydrous melts now quenched to glass (Dick and Bullen, 1984).

Small euhedral microlites of olivine and spinel randomly dispersed within glass pockets likely represent the crystallization products of the melt quenched to silicate glass in which microlites are now included (Yaxley et al., 1997). Relatively high CaO in olivine (Fig. 3A) and TiO_2 in spinel microlites (Fig. 3D) are consistent with this interpretation (Dick and Bullen, 1984). High Mg# values of olivine microlites (90.0–92.5) support their precipitation from a primitive

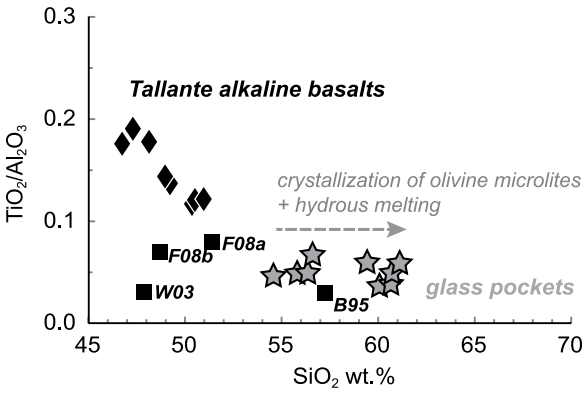

Figure 10. TiO_2/Al_2O_3 versus SiO_2 (wt%) for glasses in spinel lherzolites from Tallante in southeast Spain (gray stars) compared with data of host alkali basalts (black diamonds, Duggen et al., 2005) and experimentally determined near-solidus melts of lherzolites at 1 GPa (B95—Baker et al., 1995; F08a—Falloon et al., 2008), 1.5 GPa (F08b—Falloon et al., 2008), and of depleted harzburgite at 1 GPa (W03—Wasylenki et al., 2003) (black squares).

mantle melt that experienced minor fractional crystallization. This interpretation is consistent with experimental results that show how highly silicic mantle melts may reach saturation in high-Mg# olivine at relatively low pressure (1 GPa) (Draper and Green, 1997). Fractional crystallization of olivine likely contributed to increase SiO_2 (Fig. 10) and decrease MgO and FeO in the coexisting melt, accounting for the compositional variability of these glasses (Table S1). In the context of the petrological evolution of the Tallante peridotites, in situ low degrees of partial melting of metasomatic clinopyroxene and spinel are likely the results of supply of heat and volatiles from the Pliocene alkaline magmas that finally carried the xenoliths to the surface.

Fingerprinting the Origin of BMS Included in Metasomatic Pyroxene

All the BMS grains identified in the Tallante xenoliths are included in metasomatic pyroxene and exhibit rounded morphology (Figs. 2 and 4). This suggests that BMS are the solidified products of immiscible droplets of sulfide melt entrained in subalkaline silicate melts (e.g., Andersen et al., 1987) that produced the refertilization of Tallante peridotites via formation of clinopyroxene + orthopyroxene + spinel assemblages (Aulbach et al., 2021).

These sulfide inclusions consist of Ni-rich pentlandite coexisting with minor chalcopyrite and/or bornite (Fig. 4). At the temperature conditions (850–1050 °C) estimated for the equilibration of this set of mantle xenoliths (Hidas et al., 2016), phase relations in the Fe-Ni-Cu-S system predict that Fe-rich monosulfide solid solution (mss) should be the first solid to crystallize from sulfide melt droplets (Kullerud et al., 1969). If so, the fractionation of such sulfide melts must be governed by the sequential crystallization of monosulfide (mss) and/or intermediate (iss) [$(Cu_{1 \pm x}Fe_{1 \pm y})S_2$] solid solutions (Ballhaus et al., 2001). In this scenario, pentlandite may crystallize either at ~865 °C as a result of peritectic reaction between Fe-rich mss (pyrrhotite) and residual Ni-rich liquid (Sugaki and Kitakaze, 1998), or at a lower temperature (<610 °C) as the subsolidus re-equilibration product of former mss reacting with heazlewoodite [$(Ni, Fe)_{3 \pm x}S_2$] solid solution (hzss) (Kullerud et al., 1969). However, such a crystallization pathway does not explain the compositions of BMS from Tallante because: (1) their reconstructed bulk compositions have Cu contents (up to 14.8 wt%) exceeding the solubility limit of Cu in mss (maximum of 7.5 wt% Cu in mss structure at 935 °C; Cabri, 1973), and (2) pyrrhotite (the low temperature product of equilibration of the high-temperature mss) does not occur in our composite sulfide inclusions, ruling out the formation of pentlandite by re-equilibration of former mss, either by subsolidus or peritectic reaction (Mansur et al., 2019).

Conversely, the reconstructed bulk compositions of these sulfides point out that their parental melts had compositions arising from the central portion of the Fe-Ni-Cu-S tetrahedron (see fig. 1A in Peregoedova and Ohnenstetter, 2002) as is typical for sulfides precipitated from metasomatic Cu-(Ni-Fe)-rich melt formed by incongruent melting of pre-existing Fe-Ni-Cu sulfides (Bockrath et al., 2004; Luguet and Reisberg, 2016). The bulk Ni-Cu rich compositions, together with high metal/S (~1.1, Table S2) and low Fe/(Fe + Cu) ratios of the Tallante sulfides (Fig. 11), are more consistent with their formation in a portion of the Fe-Ni-Cu-S system dominated by the early (850–900 °C) crystallization of the quaternary solid solution comprising the compositional range between hzss and iss solid solutions (Peregoedova and Ohnenstetter, 2002). Once cooling, this quaternary solid solution may increase its bulk Ni/Cu ratio breaking down to pentlandite from hzss at ~760 °C and chalcopyrite (and/or bornite) from iss below 557 °C (Fleet and Pan, 1994; Kullerud et al., 1969; Peregoedova and Ohnenstetter, 2002), explaining the observed pn ± cp ± bn assemblages in the Tallante peridotites (Fig. 4).

On the other hand, BMS from Tallante exhibit broad variability of chondrite-normalized PGE patterns ($0.14 < Pd_N/Ir_N < 30.74$) (Fig. 9), which can be grouped into three main types: (1) sulfides with nearly chondritic PGE relative abundances ($Pd_N/Ir_N \sim 1$), which are commonly observed in "pristine" mantle mss (Bockrath et al., 2004); (2) sulfides with negatively trending PGE patterns ($Pd_N/Ir_N < 1$) as is typical of residual mss left after partial melting (i.e., Type 1 BMS in Luguet and Reisberg, 2016); and (3) sulfides with positively trending PGE patterns ($Pd_N/Ir_N > 5$) as those reported for BMS precipitated from metasomatic Ni-Cu rich sulfide melts migrating through the SCLM (i.e., Type 2 BMS in Luguet and Reisberg, 2016). These three types of chondrite-normalized PGE patterns characterize sulfide aggregates with almost constant Ni-Fe-Cu compositions (i.e., pn ± cp ± bn) (Fig. 5), suggesting that the fractionation of PGE was not governed by the known melt-solid and solid-solid partition coefficients at equilibrium. Moreover, these sulfides exhibit remarkably homogeneous concentrations of semi-metals (Figs. 9D–9F), which provides additional evidence that PGE abundances were not controlled by the expected chalcophile partitioning during fractionation of a sulfide melt, as commonly predicted by experimental results (Ballhaus et al., 2006) and empirical studies (Alard et al., 2000; Lorand and Alard, 2001). Furthermore, there is no correlation between Pd_N/Ir_N of BMS and indicators of silicate melt fractionation (e.g., La_N/Sm_N) in their host pyroxene (Fig. 12), suggesting that the variability in PGE systematics did not originate from variable extents of interaction with the agents of silicate metasomatism (e.g., Saunders et al., 2015; Tassara et al., 2018).

All these observations point out that Tallante BMS crystallized from Ni-Cu rich sulfide melt(s) that inherited the PGE signatures of distinct populations of pre-existing sulfides and/or PGM, each one with its own distinct PGE systematics, which melted incongruently during extraction and/or migration of silicate melts in the SCLM. Several works have shown that the PGE composition of the SCLM is highly heterogeneous at different scales (Aulbach et al., 2016; Aulbach et al., 2021), as the PGE budget is controlled by various populations of BMS and PGM recording multiple episodes of partial melting and metasomatism (González-Jiménez et al., 2014; Hughes et al., 2017; Tassara et al., 2018). As the melting region in subduction settings is normally several tens to hundreds of kilometers across and may extend to depths

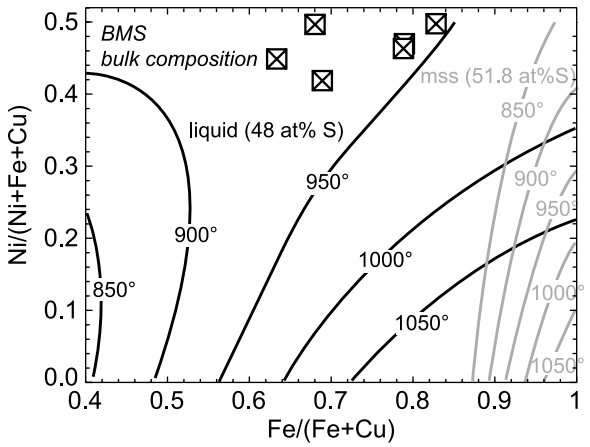

Figure 11. Reconstructed bulk compositions of base-metal sulfides (BMS) from Tallante peridotites in southeast Spain (squares) in the Fe/(Fe + Cu) versus Ni/(Ni + Fe + Cu) plot. Grey and black lines are calculated isopleths of monosulfide solid solution (mss) (51.8 at% S) and coexisting sulfide liquid (48 at% S) at different temperatures, respectively (Fleet and Pan, 1994).

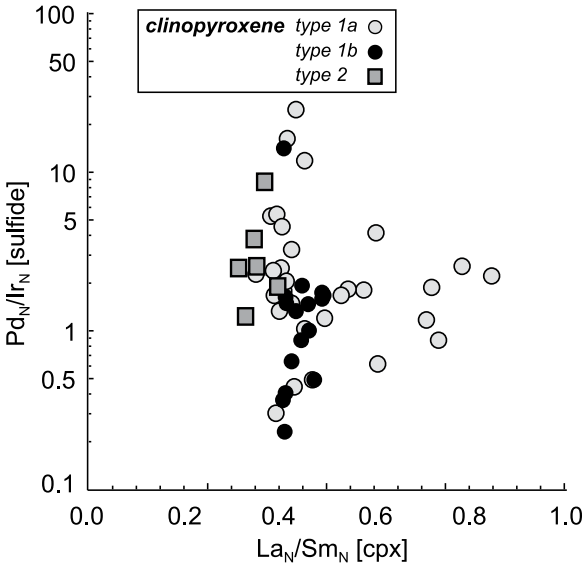

Figure 12. Pd_N/Ir_N ratio of base-metal sulfides in Tallante peridotites (southeast Spain) versus La_N/Sm_N of host clinopyroxene (cpx). Symbols as in Figure 7.

greater than 100 km (e.g., The MELT Seismic Team 1998), individual melt batches ascending through the upper mantle above a subduction zone may carry PGE signatures inherited from distinct BMS/PGM populations. The preservation of variable PGE signatures in the Tallante sulfides implies that melt extraction, melt-rock interaction, and melt crystallization did not erase the original noble metal systematics of the pre-existing sulfides and/or PGM, despite producing relatively homogeneous bulk Ni-Fe-Cu and semi-metal signatures.

The Role of Nano-to-Micrometer Sized PGM and Gold Particles

Careful examination of the time-resolved spectra signals collected during the in situ LA-ICP-MS analyses of the Tallante BMS reveals the frequent presence of ^{195}Pt, ^{108}Pd, and ^{197}Au positive spikes (Fig. 8). This observation is consistent with backscattered electron images, acquired by FEG-ESEM, confirming the presence of several types of nano-to-micrometer sized inclusions of Pt(-Pd)-Sn rich PGM (including tatyanite $Pt_9Cu_3Sn_4$, González-Jiménez et al., 2020) and gold particles in BMS (Fig. 6). The high-magnification imaging of tatyanite nanoparticles by combining high-resolution SEM and high-resolution TEM revealed a predominantly euhedral morphology and the absence of crystallographic continuity with the host BMS (i.e., pentlandite or chalcopyrite, González-Jiménez et al., 2020). These observations suggest that the formation of nano-to-micrometer sized PGM likely preceded the precipitation of their host BMS. This hypothesis is consistent with the fact that refractory Pt(-Pd)-Te-Sn compounds have higher solidus temperatures (>1200 °C) than the liquidus temperatures of Cu-Fe-Ni-S melts (Sinyakova et al., 2016, 2019), suggesting they crystallize before being trapped into BMS. The enrichment in Sn in such Pt-rich PGM (Figs. 6A and 6B) suggests that this semi-metal enhanced the formation of immiscible Pt-rich nanomelts or nanoparticles in both the silicate and sulfide liquids (Helmy et al., 2007, 2013; Anenburg and Mavrogenes, 2020; González-Jiménez et al., 2019, 2020). Interestingly, (sub)-micrometer sized PGM consisting of Pt bounded with semi-metals (As, Te, Bi) have been reported in other mantle BMS, including pentlandite (Luguet et al., 2007; Lorand et al., 2010; Alard et al., 2011; González-Jiménez et al., 2019). Experimental works also support the more refractory nature of these Pt-rich minerals than BMS, owing to the strong tendency of Pt to form semi-metal complexes in both silicate and sulfide melts (Helmy et al., 2013; Helmy and Bragagni, 2017; Anenburg and Mavrogenes, 2020).

Similarly, gold particles in the Tallante peridotites also exhibit euhedral morphology and no specific microstructure that might control their location within the host BMS, suggesting that they crystallized prior to BMS rather than by low-temperature exsolution. Previous works have shown that gold is almost insoluble into pentlandite (Piña et al., 2012) or its potential precursors such as mss, hzss, or iss (Barnes et al., 2006; Holwell et al., 2015). Indeed, Sinyakova et al. (2019) synthetized nano-to-micrometer sized gold alloys at high temperatures (>1000 °C) directly from Ni-Cu-Fe sulfide melts, demonstrating that, if these types of melts become sufficiently enriched in gold, this metal can form its own mineral phases instead of being trapped in the lattice of BMS. Moreover, experimental studies have shown that gold solubility in silicate melts is strongly related to melt sulfur content (Li and Audétat, 2013; Li et al., 2019). Therefore, once a fractionating silicate melt achieves sulfide saturation, a rapid drop in $S_{[melt]}$ may cause local precipitation of native gold, as supported by the occurrence of several gold-bearing silicate glasses in mantle xenoliths worldwide (Tassara et al., 2017; González-Jiménez et al., 2020).

An attentive analysis of the LA-ICP-MS signals of BMS indicates that negative Pt and Au anomalies in chondrite-normalized PGE patterns (Fig. 9) are systematically associated with lack of positive spikes in their respective time-resolved spectra. In contrast, positive anomalies and/or nearly chondritic proportions of Pt and Au relative to adjacent PGEs (Fig. 9) are systematically correlated with pronounced Pt and Au spikes in the time-resolved spectra (Fig. 8), confirming that the presence or absence of (sub)-micrometric particles largely controls the Pt-Au budget of the BMS. These observations suggest that a selective uptake of Pt and Au by nanoparticles (or nanomelts) preceding the formation of the Tallante BMS may have strongly depleted these two elements in the crystallizing sulfides, whereas the mechanical assimilation of these pre-existing metal particles produced nearly chondritic or superchondritic concentrations. Thus, the presence or lack of PGM and metal-bearing particles exerted a strong "disturbing impact" on the PGE systematics of the analyzed BMS.

Our interpretation confirms recent experimental (Anenburg and Mavrogenes, 2020) and empirical works (Zelenski et al., 2017; Kamenetsky and Zelenski, 2020), showing that mantle-derived sulfide droplets may preserve their variable PGE systematics over distances covering the whole lithospheric column, especially whether they transport discrete nano-to-micrometer sized particles or melts. As discussed above, the metal-bearing particles may have been segregated at any stage of the evolution of the Tallante peridotites, either directly from silicate melt prior to sulfide saturation, or from droplets of immiscible sulfide melt, once sulfide saturation was already achieved. Alternatively, Pt-rich PGM and Au-bearing minerals may have been also assimilated and transported in the silicate melt during melt extraction and migration in the SCLM in the form of solid nanoparticles or nanomelts (González-Jiménez et al., 2019, 2020; Kamenetsky and Zelenski).

METALLOGENIC MODEL

The peculiar position of the Tallante volcanic field, in the western Mediterranean, provides a perspective onto the evolution of a transitional lithospheric mantle sector between southern

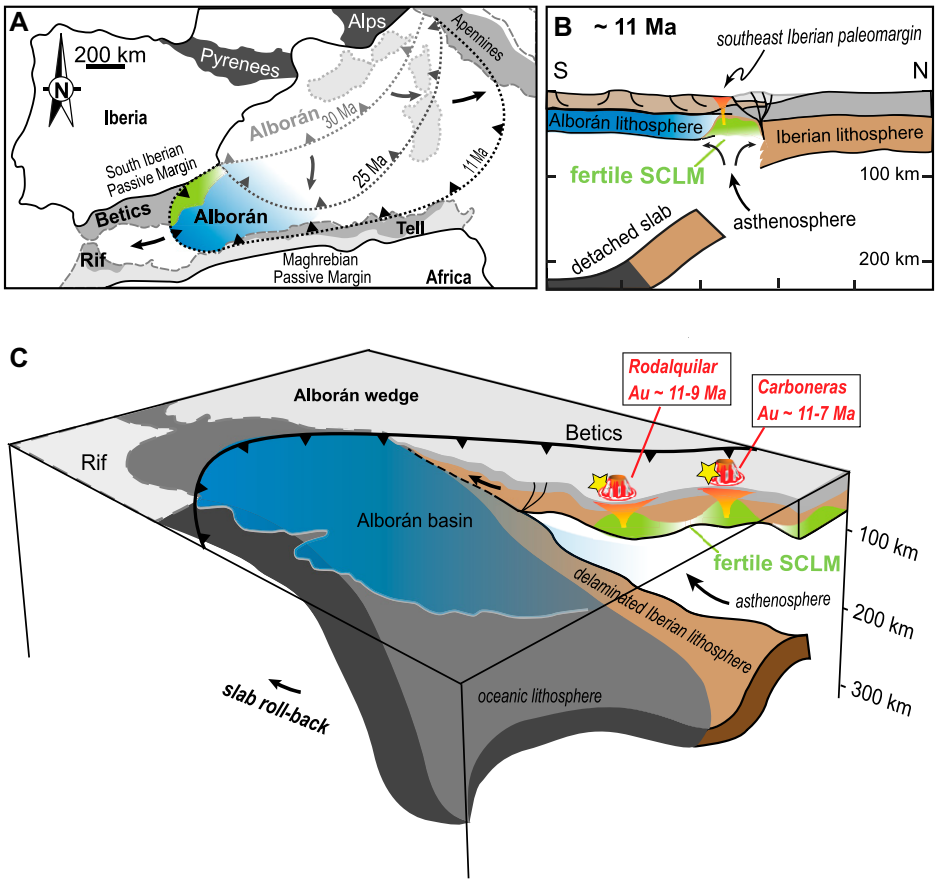

Figure 13. (A) Cartoon of the geotectonic evolution of the western Mediterranean in response to westward migration of the Alborán micro-continent in the Cenozoic. (B) N-S cross-section close to the southeast Iberian margin, as inferred by seismic profiles in Mancilla et al. (2015, 2018). (C) Conceptual 3-D geodynamic sketch of the lithospheric architecture beneath the western Mediterranean (modified after Mancilla et al., 2015). SCLM—subcontinental lithospheric mantle.

Iberia and the westward migrating Alborán micro-continent (Figs. 13A and 13B). Fertile spinel lherzolites from Tallante sampled volumes of subcontinental lithospheric mantle affected by pervasive crystallization of metasomatic sulfide-hosting pyroxenes. This refertilization event was due to the percolation of subalkaline subduction-related magmas generated by upwelling of hot mantle asthenosphere upon slab rollback and tearing of the Iberian continental lithosphere during the Miocene. Subvertical translithospheric STEP faults, which accommodated the lateral propagation of slab rupture, likely provided preferential pathways for the upward migration of silicate melts and the generation of metasomatized domains in the SCLM underlying the southern Iberian margin. The precipitation of Ni-Cu rich BMS with strongly heterogeneous PGE systematics (Fig. 9), Pt-Pd-rich PGM, and Au-bearing microinclusions (Fig. 6) hosted in the metasomatic (clinopyroxene + orthopyroxene + spinel) assemblages (Figs. 2 and 4) suggests that ascending silicate melts incorporated different populations of sulfide droplets and metal nanoparticles, which were finally concentrated in the shallower domains of the SCLM by melt-rock reaction at decreasing melt volumes. The possible presence of pyroxenites in the mantle source of these silicate melts (Marchesi et al., 2017) may have enhanced their Au budget, as pyroxenites are considered relevant sources of gold in the mantle (Saunders et al., 2018).

Precipitation of metasomatic sulfides, PGM, and metal nanoparticles provided an efficient mechanism for the storage of metals, in particular gold, in the SCLM beneath the southern Iberian margin. Indeed, BMS in Tallante peridotites have Au concentrations (median 1.78 ppm) up to 4–5 times higher than Au abundances in BMS from other xenoliths of common oceanic or continental mantle (~0.02 ppm in intraplate oceanic mantle; 0.01–0.28 ppm in depleted cratonic mantle; 0.20–0.414 ppm in metasomatized SCLM; see references in Fig. 14). Similarly to the SCLM beneath southern Patagonia (Tassara et al., 2018), high contents of Au in BMS from Tallante are linked to the presence of Au-metallogenic provinces in the upper crust (Fig. 1). This observation suggests a close link between Au abundances in mantle BMS and the metallogenic fertility of the overlying crust, supporting previous evidence of the key contribution of the metasomatized lithospheric mantle as a source of gold endowment in the upper crust (McInnes et al., 1999; Hronsky et al., 2012; Griffin et al., 2013; Tassara et al., 2017; Holwell et al., 2019; Wang et al., 2020). In this scenario, the fertile domains of SCLM sampled by sulfide-bearing Tallante peridotites may have sourced the parental magmas of middle- to high-K calc-alkaline volcanic suites genetically related to gold mineralizations in southeast Spain (Fig. 13C). The occurrence of gold magmatic particles in lamproitic dykes of the NVP (Toscani, 1999) further supports the presence of Au-rich domains in the SCLM beneath the southern Iberian margin. Gold fertility of magmas from this sector of SCLM was enhanced by relatively low melting temperature of the sulfide-bearing metasomatic assemblages, as well as by low thermal stability of their gold repositories (Ni-Cu rich BMS). Melting of fertile SCLM occurred in response to continuous asthenosphere upwelling and continental edge delamination of the Iberian lithosphere since the middle Miocene, driving the generation of ore-productive volcanic suites, progressively shifting from calc-alkaline to alkaline affinities. Such a metallogenic evolution may account for other regional settings related to the emplacement of Cu-Au deposits associated to post-subduction calc-alkaline to alkaline magmas sourced from subduction-metasomatized lithospheric mantle (Richards, 2009; Fiorentini et al., 2018; Holwell et al., 2019; Rabayrol and Hart, 2021).

In conclusion, the modification of the SCLM during the subduction-related Miocene evolution of the western Mediterranean impacted on the metallogenesis of its overlying crust by a two-stage process: (1) subalkaline silicate metasomatism efficiently stored metals, especially Au, in fertile domains of the SCLM beneath the southern Iberian margin by the precipitation of sulfide-bearing metasomatic pyroxenes during the Miocene; (2) partial melting of these fertile domains in response to continental edge delamination and asthenosphere upwelling transferred their metal budget to calc-alkaline magmas feeding mineralization and gold endowment in the overlying crust (Fig. 13). Regardless of the metasomatizing agent, the two-stage process documented here, which is at the core of the metallogenic enrichment of the western Mediterranean lithospheric domain, is akin to the one that was recently documented and numerically modeled in the Ivrea

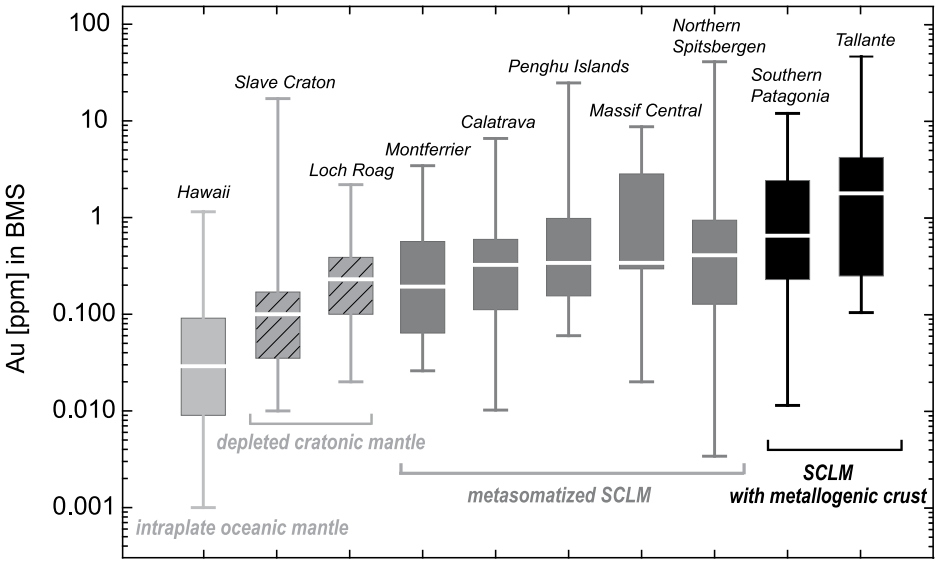

Figure 14. Box plots showing the concentrations of gold (ppm) in base-metal sulfides (BMS) of peridotite xenoliths from oceanic and continental mantle. The box depicts the central part of the sampling distribution, between the 25th and 75th percentile. The line across the box displays the median value of the distribution. Lines extending from the box represent the range of the observed values. Data sources are from Sen et al. (2010) (intraplate oceanic mantle, light gray boxes); Aulbach et al. (2004) and Hughes et al. (2017) (depleted cratonic mantle, striped gray boxes); Alard et al. (2011), González-Jiménez et al. (2014), Wang et al. (2009), Lorand and Alard (2001), and Saunders et al. (2015) (metasomatized subcontinental lithospheric mantle [SCLM], gray boxes); Tassara et al. (2018) and this study (Tallante, southeast Spain) (SCLM with metallogenic crust, black boxes).

Zone of NW Italy (Fiorentini et al., 2018). It is proposed that a two-stage process, characterized by metal-volatile enrichment and subsequent focused reactivation, may represent the most important first-order control on the localization of world-class mineralized camps worldwide.

CONCLUSIONS

Fertile spinel lherzolites from Tallante (eastern Betic Cordillera, southeast Spain) document the percolation of Miocene subalkaline silicate melts in the SCLM beneath the southern Iberian margin, which caused the crystallization of metasomatic sulfide-hosting clinopyroxene, orthopyroxene, and spinel. In the Pliocene, these sulfide-bearing metasomatic assemblages underwent small-scale partial melting in response to the influx of heat/volatiles from host alkali magmas shortly before xenolith ascent, producing interstitial silicate glass associated with spongy coronae around clinopyroxene and spinel.

Base-metal sulfides (pentlandite ± chalcopyrite ± bornite) in the Tallante peridotites represent the breakdown product of quaternary (Ni-Fe-Cu-S) sulfide solution between heazlewoodite and intermediate solid solutions, which originally precipitated from Ni-Cu-rich sulfide melts. Incongruent melting of monosulfide solid solution produced these melts during extraction and transport of the silicate magmas that finally precipitated the sulfide-hosting pyroxenes. Despite sharing homogeneous compositions in terms of major elements and semi-metals, BMS have a wide variability of PGE systematics inherited from distinct populations of sulfides and/or PGM during melting and melt percolation to the shallower SCLM. The early magmatic segregation of (sub)-micrometric PGM and metal particles, either from silicate or sulfide melts, controlled the noble metal distribution (especially of Pt and Au) in BMS, depending on whether they were incorporated or not within sulfides. Overall, BMS in Tallante peridotites have remarkably higher Au abundances than BMS in oceanic or continental mantle not associated with metallogenic crustal provinces. It is proposed that metasomatic crystallization of sulfide-hosting pyroxene provided an efficient mechanism for the storage of metals, especially Au, in this sector of SCLM underlying the ore-productive continental margin of southeast Iberia. Partial melting of this fertile source region, during progressive asthenosphere upwelling and continental edge delamination, may have effectively fed the metal cargoes of the calc-alkaline volcanism genetically associated with ore mineralization in the upper crust.

ACKNOWLEDGMENTS

We thank the Associate Editor W.U. Reimold, and the referees T. Jalowitzki and M.L. Fiorentini for their constructive reviews of the submitted version of the manuscript. This research was supported by the BES-2017-079949 Ph.D. fellowship to ES. The Spanish projects PID2019-111715GB-I00/AEI/10.13039/501100011033 and RTI2018-099157-A-I00 provided funding for field emission gun–environmental scanning electron microscopy (FEG-ESEM) and electron microprobe microanalyses (EMPA)/laser ablation–inductively coupled plasma–mass spectrometry (LA-ICP-MS) analyses of sulfides, respectively, while the Junta de Andalucía project FUMESA B-RNM-189-UGR18 financed LA-ICP-MS analyses of silicates. Research grants, infrastructures, and human resources leading to this research have benefited from funding by the European Social Fund and the European Regional Development Fund. We thank Jesús Montes Rueda (Universidad de Granada), Isabel Sánchez Almazo (Centro de Instrumentación Cientifica [CIC], Universidad de Granada), Xavier Llovet (Centres Científics i Tecnològics, Universitat de Barcelona), Miguel Ángel Hidalgo Laguna (CIC, Universidad de Granada), and Manuel Jesús Román Alpiste (Instituto Andaluz de Ciencias de la Tierra, Consejo Superior de Investigaciones Científicas-Universidad de Granada) for their careful technical assistance during sample preparation, FEG-ESEM, electron microprobe analyzes, and LA-ICP-MS analyses, respectively.

REFERENCES CITED

Alard, O., Griffin, W.L., Lorand, J.P., Jackson, S.E., and O'Reilly, S.Y., 2000, Non-chondritic distribution of the highly siderophile elements in mantle sulphides: Nature, v. 407, p. 891–894, https://doi.org/10.1038/35038049.

Alard, O., Lorand, J.P., Reisberg, L., Bodinier, J.L., Dautria, J.M., and O'Reilly, S.Y., 2011, Volatile-rich metasomatism in Montferrier xenoliths (Southern France): Implications for the abundances of chalcophile and highly siderophile elements in the subcontinental mantle: Journal of Petrology, v. 52, p. 2009–2045, https://doi.org/10.1093/petrology/egr038.

Andersen, T., Griffin, W.L., and O'Reilly, S.Y., 1987, Primary sulphide melt inclusions in mantle-derived megacrysts and pyroxenites: Lithos, v. 20, p. 279–294, https://doi.org/10.1016/S0024-4937(87)80002-6.

Anenburg, M., and Mavrogenes, J.A., 2020, Noble metal nanonugget insolubility in geological sulfide liquids: Geology, v. 48, p. 939–943, https://doi.org/10.1130/G47579.1.

Arribas, A., Cunningham, C.G., Rytuba, J.J., Rye, R.O., Kelly, W.C., Podwysocki, M.H., McKee, E.H., and Tosdal, R.M., 1995, Geology, geochronology, fluid inclusions, and isotope geochemistry of the Rodalquilar gold alunite deposit, Spain: Economic Geology and the Bulletin of the Society of Economic Geologists, v. 90, p. 795–822, https://doi.org/10.2113/gsecongeo.90.4.795.

Aulbach, S., Griffin, W.L., Pearson, N.J., O'Reilly, S.Y., Kivi, K., and Doyle, B.J., 2004, Mantle formation and evolution, Slave Craton: Constraints from HSE abundances and Re-Os isotope systematics of sulfide inclusions in mantle xenocrysts: Chemical Geology, v. 208, p. 61–88, https://doi.org/10.1016/j.chemgeo.2004.04.006.

Aulbach, S., Mungall, J.E., and Pearson, D.G., 2016, Distribution and processing of highly siderophile elements in cratonic mantle lithosphere: Reviews in Mineralogy and Geochemistry, v. 81, p. 239–304, https://doi.org/10.2138/rmg.2016.81.5.

Aulbach, S., Giuliani, A., Fiorentini, M.L., Baumgartner, R.J., Savard, D., Kamenetsky, V.S., Caruso, S., Danyushevky, L.V., Powell, W., and Griffin, W.L., 2021, Siderophile and chalcophile elements in spinels, sulphides and native Ni in strongly metasomatised xeno-

liths from the Bultfontein kimberlite (South Africa): Lithos, v. 380–381, p. 105880, https://doi.org/10.1016/j.lithos.2020.105880.

Baker, M.B., Hirschmann, M.M., Ghiorso, M.S., and Stolper, E.M., 1995, Compositions of near-solidus peridotite melts from experiments and thermodynamic calculations: Nature, v. 375, p. 308–311, https://doi.org/10.1038/375308a0.

Ballhaus, C., Tredoux, M., and Späth, A., 2001, Phase relations in the Fe-Ni-Cu-PGE-S system at magmatic temperature and application to massive sulphide ores of the Sudbury igneous complex: Journal of Petrology, v. 42, p. 1911–1926, https://doi.org/10.1093/petrology/42.10.1911.

Ballhaus, C., Bockrath, C., Wohlgemuth-Ueberwasser, C., Laurenz, V., and Berndt, J., 2006, Fractionation of the noble metals by physical processes: Contributions to Mineralogy and Petrology, v. 152, p. 667–684, https://doi.org/10.1007/s00410-006-0126-z.

Barnes, S.J., Cox, R.A., and Zientek, M.L., 2006, Platinum-group element, gold, silver and base metal distribution in compositionally zoned sulfide droplets from the Medvezky Creek Mine, Noril'sk, Russia: Contributions to Mineralogy and Petrology, v. 152, p. 187–200, https://doi.org/10.1007/s00410-006-0100-9.

Beccaluva, L., Bianchini, G., Bonadiman, C., Siena, F., and Vaccaro, C., 2004, Coexisting anorogenic and subduction-related metasomatism in mantle xenoliths from the Betic Cordillera (southern Spain): Lithos, v. 75, p. 67–87, https://doi.org/10.1016/j.lithos.2003.12.015.

Bedini, R.M., Bodinier, J.L., Dautria, J.M., and Morten, L., 1997, Evolution of LILE-enriched small melt fractions in the lithospheric mantle: A case study from the East African Rift: Earth and Planetary Science Letters, v. 153, p. 67–83, https://doi.org/10.1016/S0012-821X(97)00167-2.

Bezada, M.J., Humphreys, E.D., Toomey, D.R., Harnafi, M., Dávila, J.M., and Gallart, J., 2013, Evidence for slab rollback in westernmost Mediterranean from improved upper mantle imaging: Earth and Planetary Science Letters, v. 368, p. 51–60, https://doi.org/10.1016/j.epsl.2013.02.024.

Bianchini, G., Beccaluva, L., Nowell, G.M., Pearson, D.G., and Siena, F., 2011, Mantle xenoliths from Tallante (Betic Cordillera): Insights into the multistage evolution of the south Iberian lithosphere: Lithos, v. 124, p. 308–318, https://doi.org/10.1016/j.lithos.2010.12.004.

Bianchini, G., Braga, R., Langone, A., Natali, C., and Tiepolo, M., 2015, Metasedimentary and igneous xenoliths from Tallante (Betic Cordillera, Spain): Inferences on crust-mantle interactions and clues for post-collisional volcanism magma sources: Lithos, v. 220, p. 191–199, https://doi.org/10.1016/j.lithos.2015.02.011.

Bierlein, F.P., Groves, D.I., and Cawood, P.A., 2009, Metallogeny of accretionary orogens: The connection between lithospheric processes and metal endowment: Ore Geology Reviews, v. 36, p. 282–292, https://doi.org/10.1016/j.oregeorev.2009.04.002.

Blanks, D.E., Holwell, D.A., Fiorentini, M.L., Moroni, M., Giuliani, A., Tassara, S., González-Jiménez, J.M., Boyce, A.J., and Ferrari, E., 2020, Fluxing of mantle carbon as a physical agent for metallogenic fertilization of the crust: Nature Communications, v. 11, p. 1–11, https://doi.org/10.1038/s41467-020-18157-6.

Bockrath, C., Ballhaus, C., and Holzheid, A., 2004, Fractionation of the platinum-group elements during mantle melting: Science, v. 305, p. 1951–1953, https://doi.org/10.1126/science.1100160.

Cabri, L.J., 1973, New data on phase relations in the Cu-Fe-S system: Economic Geology and the Bulletin of the Society of Economic Geologists, v. 68, p. 443–454, https://doi.org/10.2113/gsecongeo.68.4.443.

Chong, J., Fiorentini, M.L., Holwell, D.A., Moroni, M., Blanks, D.E., Dering, G.M., Davis, A., and Ferrari, E., 2021, Magmatic cannibalisation of a Permo-Triassic Ni-Cu-PGE-(Au-Te) system during the breakup of Pangea: Implications for craton margin metal and volatile transfer in the lower crust: Lithos, v. 388–389, no. 106079, https://doi.org/10.1016/j.lithos.2021.106079.

Coltorti, M., Beccaluva, L., Bonadiman, C., Salvini, L., and Siena, F., 2000, Glasses in mantle xenoliths as geochemical indicators of metasomatic agents: Earth and Planetary Science Letters, v. 183, p. 303–320, https://doi.org/10.1016/S0012-821X(00)00274-0.

Dick, H.J., and Bullen, T., 1984, Chromian spinel as a petrogenetic indicator in abyssal and alpine-type peridotites and spatially associated lavas: Contributions to Mineralogy and Petrology, v. 86, p. 54–76, https://doi.org/10.1007/BF00373711.

Draper, D.S., and Green, T.H., 1997, P-T phase relations of silicic, alkaline, aluminous mantle-xenolith glasses under anhydrous and C-O-H fluid-saturated conditions: Journal of Petrology, v. 38, p. 1187–1224, https://doi.org/10.1093/petroj/38.9.1187.

Duggen, S., Hoernle, K., van den Bogaard, P., and Harris, C., 2004, Magmatic evolution of the Alboran region: The role of subduction in forming the western Mediterranean and causing the Messinian Salinity Crisis: Earth and Planetary Science Letters, v. 218, p. 91–108, https://doi.org/10.1016/S0012-821X(03)00632-0.

Duggen, S., Hoernle, K., van den Bogaard, P., and Garbe-Schönberg, D., 2005, Post-collisional transition from subduction-to intraplate-type magmatism in the westernmost Mediterranean: Evidence for continental-edge delamination of subcontinental lithosphere: Journal of Petrology, v. 46, p. 1155–1201, https://doi.org/10.1093/petrology/egi013.

Duggen, S., Hoernle, K., Klügel, A., Geldmacher, J., Thirlwall, M., Hauff, F., Lowry, D., and Oates, N., 2008, Geochemical zonation of the Miocene Alborán Basin volcanism (westernmost Mediterranean): Geodynamic implications: Contributions to Mineralogy and Petrology, v. 156, p. 577–593, https://doi.org/10.1007/s00410-008-0302-4.

Esteban-Arispe, I., Velasco, F., Boyce, A.J., Morales-Ruano, S., Yusta, I., and Carrillo-Rosúa, J., 2016, Unconventional non-magmatic sulfur source for the Mazarrón Zn-Pb-Cu-Ag-Fe epithermal deposit (SE Spain): Ore Geology Reviews, v. 72, p. 1102–1115, https://doi.org/10.1016/j.oregeorev.2015.10.005.

Falloon, T.J., Green, D.H., Danyushevsky, L.V., and McNeill, A.W., 2008, The composition of near-solidus partial melts of fertile peridotite at 1 and 1.5 GPa: Implications for the petrogenesis of MORB: Journal of Petrology, v. 49, p. 591–613, https://doi.org/10.1093/petrology/egn009.

Fiorentini, M.L., LaFlamme, C., Denyszyn, S., Mole, D., Maas, R., Locmelis, M., Caruso, S., and Bui, T.-H., 2018, Post-collisional alkaline magmatism as gateway for metal and sulfur enrichment of the continental lower crust: Geochimica et Cosmochimica Acta, v. 223, p. 175–197, https://doi.org/10.1016/j.gca.2017.11.009.

Fischer-Gödde, M., Becker, H., and Wombacher, F., 2010, Rhodium, gold and other highly siderophile element abundances in chondritic meteorites: Geochimica et Cosmochimica Acta, v. 74, p. 356–379, https://doi.org/10.1016/j.gca.2009.09.024.

Fleet, M.E., and Pan, Y., 1994, Fractional crystallization of anhydrous sulfide liquid in the system Fe-Ni-Cu-S, with application to magmatic sulfide deposits: Geochimica et Cosmochimica Acta, v. 58, p. 3369–3377, https://doi.org/10.1016/0016-7037(94)90092-2.

Gaetani, G.A., and Grove, T.L., 1998, The influence of water on melting of mantle peridotite: Contributions to Mineralogy and Petrology, v. 131, p. 323–346, https://doi.org/10.1007/s004100050396.

Gómez-Pugnaire, M.T., Sánchez-Vizcaíno, V.L., Fernández-Soler, J.M., and Acosta-Vigil, A., 2019, Mesozoic and Cenozoic magmatism in the Betics, *in* Quesada C., and Oliveira J., eds., The Geology of Iberia: A Geodynamic Approach: Cham, Switzerland, Springer, p. 545–566, https://doi.org/10.1007/978-3-030-11295-0_14.

González-Jiménez, J.M., Villaseca, C., Griffin, W.L., O'Reilly, S.Y., Belousova, E., Ancochea, E., and Pearson, N.J., 2014, Significance of ancient sulfide PGE and Re-Os signatures in the mantle beneath Calatrava, Central Spain: Contributions to Mineralogy and Petrology, v. 168, no. 1047, https://doi.org/10.1007/s00410-014-1047-x.

González-Jiménez, J.M., Roqué-Rosell, J., Jiménez-Franco, A., Tassara, S., Nieto, F., Gervilla, F., Baurier, S., Proenza, J.A., Saunders, E., Deditius, A.P., Schilling, M., and Corgne, A., 2019, Magmatic platinum nanoparticles in metasomatic silicate glasses and sulfides from Patagonian mantle xenoliths: Contributions to Mineralogy and Petrology, v. 174, no. 47, https://doi.org/10.1007/s00410-019-1583-5.

González-Jiménez, J.M., Tassara, S., Schettino, E., Roqué-Rosell, J., Farré-de-Pablo, J., Saunders, J.E., Deditius, A.P., Colás, V., Rovira-Medina, J.J., Guadalupe-Dávalos, M., Schilling, M., Jimenez-Franco, A., Marchesi, C., Nieto, F., Proenza, J.A., and Gervilla, F., 2020, Mineralogy of the HSE in the subcontinental lithospheric mantle: An interpretive review: Lithos, v. 372, no. 105681, https://doi.org/10.1016/j.lithos.2020.105681.

Griffin, W.L., Begg, G.C., and O'Reilly, S.Y., 2013, Continental-root control on the genesis of magmatic ore deposits: Nature Geoscience, v. 6, p. 905–910, https://doi.org/10.1038/ngeo1954.

Groves, D.I., Zhang, L., and Santosh, M., 2020, Subduction, mantle metasomatism, and gold: A dynamic and genetic conjunction: Geological Society of America Bulletin, v. 132, p. 1419–1426, https://doi.org/10.1130/B35379.1.

Helmy, H.M., and Bragagni, A., 2017, Platinum-group elements fractionation by selective complexing, the Os, Ir, Ru, Rh-arsenide-sulfide systems above 1020° C: Geochimica et Cosmochimica Acta, v. 216, p. 169–183, https://doi.org/10.1016/j.gca.2017.01.040.

Helmy, H.M., Ballhaus, C., Berndt, J., Bockrath, C., and Wohlgemuth-Ueberwasser, C., 2007, Formation of Pt, Pd and Ni tellurides: Experiments in sulfide-telluride systems: Contributions to Mineralogy and Petrology, v. 153, p. 577–591, https://doi.org/10.1007/s00410-006-0163-7.

Helmy, H.M., Ballhaus, C., Fonseca, R.O., Wirth, R., Nagel, T., and Tredoux, M., 2013, Noble metal nanoclusters and nanoparticles precede mineral formation in magmatic sulphide melts: Nature Communications, v. 4, no. 2405, https://doi.org/10.1038/ncomms3405.

Hidas, K., Konc, Z., Garrido, C.J., Tommasi, A., Vauchez, A., Padrón-Navarta, J.A., Marchesi, C., Booth-Rea, G., Acosta-Vigil, A., Szabó, C., Varas-Reus, M.I., and Gervilla, F., 2016, Flow in the western Mediterranean shallow mantle: Insights from xenoliths in Pliocene alkali basalts from SE Iberia (eastern Betics, Spain): Tectonics, v. 35, p. 2657–2676, https://doi.org/10.1002/2016TC004165.

Holwell, D.A., Keays, R.R., McDonald, I., and Williams, M.R., 2015, Extreme enrichment of Se, Te, PGE and Au in Cu sulfide microdroplets: evidence from LA-ICP-MS analysis of sulfides in the Skaergaard Intrusion, east Greenland: Contributions to Mineralogy and Petrology, v. 170, no. 53, https://doi.org/10.1007/s00410-015-1203-y.

Holwell, D.A., Fiorentini, M., McDonald, I., Lu, Y., Giuliani, A., Smith, D.J., Keith, M., and Locmelis, M., 2019, A metasomatized lithospheric mantle control on the metallogenic signature of post-subduction magmatism: Nature Communications, v. 10, p. 1–10, https://doi.org/10.1038/s41467-019-11065-4.

Hronsky, J.M., Groves, D.I., Loucks, R.R., and Begg, G.C., 2012, A unified model for gold mineralisation in accretionary orogens and implications for regional-scale exploration targeting methods: Mineralium Deposita, v. 47, p. 339–358, https://doi.org/10.1007/s00126-012-0402-y.

Hughes, H.S., McDonald, I., Loocke, M., Butler, I.B., Upton, B.G., and Faithfull, J.W., 2017, Paradoxical co-existing base metal sulphides in the mantle: The multi-event record preserved in Loch Roag peridotite xenoliths, North Atlantic Craton: Lithos, v. 276, p. 103–121, https://doi.org/10.1016/j.lithos.2016.09.035.

Ionov, D.A., Hofmann, A.W., and Shimizu, N., 1994, Metasomatism-induced melting in mantle xenoliths from Mongolia: Journal of Petrology, v. 35, p. 753–785, https://doi.org/10.1093/petrology/35.3.753.

Ionov, D.A., Bodinier, J.L., Mukasa, S.B., and Zanetti, A., 2002, Mechanisms and sources of mantle metasomatism: Major and trace element compositions of peridotite xenoliths from Spitsbergen in the context of numerical modelling: Journal of Petrology, v. 43, p. 2219–2259, https://doi.org/10.1093/petrology/43.12.2219.

Jin, Z.M., Green, H.W., and Zhou, Y., 1994, Melt topology in partially molten mantle peridotite during ductile deformation: Nature, v. 372, p. 164–167, https://doi.org/10.1038/372164a0.

Kamenetsky, V.S., and Zelenski, M., 2020, Origin of noble-metal nuggets in sulfide-saturated arc magmas: A case study of olivine-hosted sulfide melt inclusions from the Tolbachik volcano (Kamchatka, Russia): Geology, v. 48, p. 620–624, https://doi.org/10.1130/G47086.1.

Kovács, I., Hidas, K., Hermann, J., Sharygin, V., Szabo, C., and Ntaflos, T., 2007, Fluid induced melting in mantle xenoliths and some implications for the continental lithospheric mantle from the Minusinsk Region (Khakasia, southern Siberia): Geologica Carpathica, v. 58, no. 211.

Kullerud, G., Yund, R.A., and Moh, G.H., 1969, Phase relations in the Cu-Fe-S, Cu-Ni-S and Fe-Ni-S system, *in* Wilson, H.D.B., ed., Magmatic Ore Deposits: Lancaster, Pennsylvania, USA, Economic Geology Publishing Co., p. 323–343, https://doi.org/10.5382/Mono.04.23.

Lambart, S., Laporte, D., Provost, A., and Schiano, P., 2012, Fate of pyroxenite-derived melts in the peridotitic mantle: Thermodynamic and experimental constraints: Journal of Petrology, v. 53, p. 451–476, https://doi.org/10.1093/petrology/egr068.

Li, Y., and Audétat, A., 2013, Gold solubility and partitioning between sulfide liquid, monosulfide solid solution and hydrous mantle melts: Implications for the formation of Au-rich magmas and crust-mantle differentiation: Geochimica et Cosmochimica Acta, v. 118, p. 247–262, https://doi.org/10.1016/j.gca.2013.05.014.

Li, Y., Feng, L., Kiseeva, E.S., Gao, Z., Guo, H., Du, Z., Wang, F., and Shi, L., 2019, An essential role for sulfur in sulfide-silicate melt partitioning of gold and magmatic gold transport at subduction settings: Earth and Planetary Science Letters, v. 528, no. 115850, https://doi.org/10.1016/j.epsl.2019.115850.

Lonergan, L., and White, N., 1997, Origin of the Betic-Rif mountain belt: Tectonics, v. 16, p. 504–522, https://doi.org/10.1029/96TC03937.

Lorand, J.P., and Alard, O., 2001, Platinum-group element abundances in the upper mantle: New constraints from in situ and whole-rock analyses of Massif Central xenoliths (France): Geochimica et Cosmochimica Acta, v. 65, p. 2789–2806, https://doi.org/10.1016/S0016-7037(01)00627-5.

Lorand, J.P., and Luguet, A., 2016, Chalcophile and siderophile elements in mantle rocks: Trace elements controlled by trace minerals: Reviews in Mineralogy and Geochemistry, v. 81, p. 441–488, https://doi.org/10.2138/rmg.2016.81.08.

Lorand, J.P., Luguet, A., Alard, O., Bezos, A., and Meisel, T., 2008, Abundance and distribution of platinum-group elements in orogenic lherzolites; a case study in a Fontete Rouge lherzolite (French Pyrénées): Chemical Geology, v. 248, p. 174–194, https://doi.org/10.1016/j.chemgeo.2007.06.030.

Lorand, J.P., Alard, O., and Luguet, A., 2010, Platinum-group element micronuggets and refertilization process in Lherz orogenic peridotite (northeastern Pyrenees, France): Earth and Planetary Science Letters, v. 289, p. 298–310, https://doi.org/10.1016/j.epsl.2009.11.017.

Lorand, J.P., Luguet, A., and Alard, O., 2013, Platinum-group element systematics and petrogenetic processing of the continental upper mantle: A review: Lithos, v. 164, p. 2–21, https://doi.org/10.1016/j.lithos.2012.08.017.

Luguet, A., and Reisberg, L., 2016, Highly siderophile element and 1870s signatures in non-cratonic basalt-hosted peridotite xenoliths: Unravelling the origin and evolution of the post-Archean lithospheric mantle: Reviews in Mineralogy and Geochemistry, v. 81, p. 305–367, https://doi.org/10.2138/rmg.2016.81.06.

Luguet, A., Alard, O., Lorand, J.P., Pearson, N.J., Ryan, C., and O'Reilly, S.Y., 2001, Laser-ablation microprobe (LAM)-ICPMS unravels the highly siderophile element geochemistry of the oceanic mantle: Earth and Planetary Science Letters, v. 189, p. 285–294, https://doi.org/10.1016/S0012-821X(01)00357-0.

Luguet, A., Lorand, J.P., and Seyler, M., 2003, Sulfide petrology and highly siderophile element geochemistry of abyssal peridotites: A coupled study of samples from the Kane Fracture Zone (45 W 23 20N, MARK area, Atlantic Ocean): Geochimica et Cosmochimica Acta, v. 67, p. 1553–1570, https://doi.org/10.1016/S0016-7037(02)01133-X.

Luguet, A., Shirey, S.B., Lorand, J.P., Horan, M.F., and Carlson, R.W., 2007, Residual platinum-group minerals from highly depleted harzburgites of the Lherz massif (France) and their role in HSE fractionation of the mantle: Geochimica et Cosmochimica Acta, v. 71, p. 3082–3097, https://doi.org/10.1016/j.gca.2007.04.011.

Mancilla, F. de Lis, Booth-Rea, G., Stich, D., Pérez-Peña, J.V., Morales, J., Azañón, J.M., Martín, R., and Giaconia, F., 2015, Slab rupture and delamination under the Betics and Rif constrained from receiver functions: Tectonophysics, v. 663, p. 225–237, https://doi.org/10.1016/j.tecto.2015.06.028.

Mancilla, F. de Lis, Heit, B., Morales, J., Yuan, X., Stich, D., Molina-Aguilera, A., Azañon, J.M., and Martín, R., 2018, A STEP fault in Central Betics, associated with lateral lithospheric tearing at the northern edge of the Gibraltar arc subduction system: Earth and Planetary Science Letters, v. 486, p. 32–40, https://doi.org/10.1016/j.epsl.2018.01.008.

Mansur, E.T., Barnes, S.J., and Duran, C.J., 2019, Textural and compositional evidence for the formation of pentlandite via peritectic reaction: Implications for the distribution of highly siderophile elements: Geology, v. 47, p. 351–354, https://doi.org/10.1130/G45779.1.

Marchesi, C., Dale, C.W., Garrido, C.J., Pearson, D.G., Bosch, D., Bodinier, J.L., Gervilla, F., and Hidas, K., 2014, Fractionation of highly siderophile elements in refertilized mantle: Implications for the Os isotope composition of basalts: Earth and Planetary Science Letters, v. 400, p. 33–44, https://doi.org/10.1016/j.epsl.2014.05.025.

Marchesi, C., Konc, Z., Garrido, C.J., Bosch, D., Hidas, K., Varas-Reus, M.I., and Acosta-Vigil, A., 2017, Multistage evolution of the lithospheric mantle beneath the westernmost Mediterranean: Geochemical constraints from peridotite xenoliths in the eastern Betic Cordillera (SE Spain): Lithos, v. 276, p. 75–89, https://doi.org/10.1016/j.lithos.2016.12.011.

McDonough, W.F., and Sun, S.S., 1995, The composition of the Earth: Chemical Geology, v. 120, p. 223–253, https://doi.org/10.1016/0009-2541(94)00140-4.

McInnes, B.I., McBride, J.S., Evans, N.J., Lambert, D.D., and Andrew, A.S., 1999, Osmium isotope constraints on ore metal recycling in subduction zones: Science, v. 286, p. 512–516, https://doi.org/10.1126/science.286.5439.512.

Morales-Ruano, S.M., Rosúa, F.J.C., Hach-Alí, P.F., De La Fuente Chacón, F., and López, E.C., 2000, Epithermal Cu-Au mineralization in the Palai-Islica deposit, Almeria, Southeastern Spain: Fluid-inclusion evidence for mixing of fluids as a guide to gold mineralization: Canadian Mineralogist, v. 38, p. 553–565, https://doi.org/10.2113/gscanmin.38.3.553.

Navon, O., and Stolper, E., 1987, Geochemical consequences of melt percolation: The upper mantle as a chromatographic column: The Journal of Geology, v. 95, p. 285–307, https://doi.org/10.1086/629131.

Neumann, E.R., and Wulff-Pedersen, E., 1997, The origin of highly silicic glass in mantle xenoliths from the Canary Islands: Journal of Petrology, v. 38, p. 1513–1539, https://doi.org/10.1093/petroj/38.11.1513.

O'Driscoll, B., and González-Jiménez, J.M., 2016, Petrogenesis of the platinum-group minerals: Reviews in Mineralogy and Geochemistry, v. 81, p. 489–578, https://doi.org/10.2138/rmg.2016.81.09.

Pan, S., Zheng, J., Yin, Z., Griffin, W.L., Xia, M., Lin, A., and Zhang, H., 2018, Spongy texture in mantle clinopyroxene records decompression-induced melting: Lithos, v. 320, p. 144–154, https://doi.org/10.1016/j.lithos.2018.08.035.

Peregoedova, A., and Ohnenstetter, M., 2002, Collectors of Pt, Pd and Rh in a S-poor Fe-Ni-Cu sulfide system at 760 C: Experimental data and application to ore deposits: Canadian Mineralogist, v. 40, p. 527–561, https://doi.org/10.2113/gscanmin.40.2.527.

Peregoedova, A., Barnes, S.J., and Baker, D.R., 2004, The formation of Pt-Ir alloys and Cu-Pd-rich sulfide melts by partial desulfurization of Fe-Ni-Cu sulfides: Results of experiments and implications for natural systems: Chemical Geology, v. 208, p. 247–264, https://doi.org/10.1016/j.chemgeo.2004.04.015.

Piña, R., Gervilla, F., Barnes, S.J., Ortega, L., and Lunar, R., 2012, Distribution of platinum-group and chalcophile elements in the Aguablanca Ni-Cu sulfide deposit (SW Spain): Evidence from a LA-ICP-MS study: Chemical Geology, v. 302, p. 61–75, https://doi.org/10.1016/j.chemgeo.2011.02.010.

Platt, J.P., Behr, W.M., Johanesen, K., and Williams, J.R., 2013, The Betic-Rif arc and its orogenic hinterland: A review: Annual Review of Earth and Planetary Sciences, v. 41, p. 313–357, https://doi.org/10.1146/annurev-earth-050212-123951.

Rabayrol, F., and Hart, C.J.R., 2021, Petrogenetic and tectonic controls on magma fertility and the formation of post-subduction porphyry and epithermal mineralization along the late Cenozoic Anatolian Metallogenic Trend, Turkey: Mineralium Deposita, v. 56, p. 279–306, https://doi.org/10.1007/s00126-020-00967-9.

Rampone, E., Piccardo, G.B., Vannucci, R., and Bottazzi, P., 1997, Chemistry and origin of trapped melts in ophioiitic peridotites: Geochimica et Cosmochimica Acta, v. 61, p. 4557–4569, https://doi.org/10.1016/S0016-7037(97)00260-3.

Rampone, E., Vissers, R.L.M., Poggio, M., Scambelluri, M., and Zanetti, A., 2010, Melt migration and intrusion during exhumation of the Alboran lithosphere: The Tallante mantle xenolith record (Betic Cordillera, SE Spain): Journal of Petrology, v. 51, p. 295–325, https://doi.org/10.1093/petrology/egp061.

Richards, J.P., 2009, Postsubduction porphyry Cu-Au and epithermal Au deposits: Products of remelting of subduction-modified lithosphere: Geology, v. 37, p. 247–250, https://doi.org/10.1130/G25451A.1.

Richards, J.P., 2013, Giant ore deposits formed by optimal alignments and combinations of geological processes: Nature Geoscience, v. 6, p. 911–916, https://doi.org/10.1038/ngeo1920.

Sänger-von Oepen, P., Friedrich, G., and Vogt, J.H., 1989, Fluid evolution, wallrock alteration, and ore mineralization associated with the Rodalquilar epithermal gold-deposit in southeast Spain: Mineralium Deposita, v. 24, p. 235–243, https://doi.org/10.1007/BF00206385.

Saunders, J.E., Pearson, N.J., O'Reilly, S.Y., and Griffin, W.L., 2015, Sulfide metasomatism and the mobility of gold in the lithospheric mantle: Chemical Geology, v. 410, p. 149–161, https://doi.org/10.1016/j.chemgeo.2015.06.016.

Saunders, J.E., Pearson, N.J., O'Reilly, S.Y., and Griffin, W.L., 2016, Gold in the mantle: The role of pyroxenites: Lithos, v. 244, p. 205–217, https://doi.org/10.1016/j.lithos.2015.12.008.

Saunders, J.E., Pearson, N.J., O'Reilly, S.Y., and Griffin, W.L., 2018, Gold in the mantle: A global assessment of abundance and redistribution processes: Lithos, v. 322, p. 376–391, https://doi.org/10.1016/j.lithos.2018.10.022.

Sen, I.S., Bizimis, M., and Sen, G., 2010, Geochemistry of sulfides in Hawaiian garnet pyroxenite xenoliths: Implications for highly siderophile elements in the oceanic mantle: Chemical Geology, v. 273, p. 180–192, https://doi.org/10.1016/j.chemgeo.2010.02.021.

Shimizu, Y., Arai, S., Morishita, T., and Ishida, Y., 2008, Origin and significance of spinel-pyroxene symplectite in lherzolite xenoliths from Tallante, SE Spain: Mineralogy and Petrology, v. 94, p. 27–43, https://doi.org/10.1007/s00710-008-0004-7.

Sinyakova, E., Kosyakov, V., Distler, V., and Karmanov, N., 2016, Behavior of Pt, Pd, and Au during crystallization of Cu-rich magmatic sulfide minerals: Canadian Mineralogist, v. 54, p. 491–509, https://doi.org/10.3749/canmin.1500015.

Sinyakova, E., Kosyakov, V., Palyanova, G., and Karmanov, N., 2019, Experimental modeling of noble and chalcophile elements fractionation during solidification of Cu-Fe-Ni-S melt: Minerals (Basel), v. 9, no. 531, https://doi.org/10.3390/min9090531.

Sugaki, A., and Kitakaze, A., 1998, High form of pentlandite and its thermal stability: The American

Mineralogist, v. 83, p. 133–140, https://doi.org/10.2138/am-1998-1-213.

Tassara, S., González-Jiménez, J.M., Reich, M., Schilling, M.E., Morata, D., Begg, G., Saunders, E., Griffin, W.L., O'Reilly, S.Y., Grégoire, M., Barra, F., and Corgne, A., 2017, Plume-subduction interaction forms large auriferous provinces: Nature Communications, v. 8, p. 1–7, https://doi.org/10.1038/s41467-017-00821-z.

Tassara, S., González-Jiménez, J.M., Reich, M., Saunders, E., Luguet, A., Morata, D., Grégoire, M., van Acken, D., Schilling, M.E., Barra, F., Nowell, G., and Corgne, A., 2018, Highly siderophile elements mobility in the subcontinental lithospheric mantle beneath southern Patagonia: Lithos, v. 314, p. 579–596, https://doi.org/10.1016/j.lithos.2018.06.022.

The MELT Seismic Team, 1998, Imaging the deep seismic structure beneath a mid-ocean ridge: The MELT experiment: Science, v. 280, p. 1215–1218, https://doi.org/10.1126/science.280.5367.1215.

Toscani, L., 1999, Magmatic gold grains in the El Tale lamproite, Fortuna, SE Spain: Mineralogical Magazine, v. 63, p. 595–602, https://doi.org/10.1180/minmag.1999.063.4.12.

Varas-Reus, M.I., Garrido, C.J., Marchesi, C., Bosch, D., Acosta-Vigil, A., Hidas, K., Barich, A., and Booth-Rea, G., 2017, Sr-Nd-Pb isotopic systematics of crustal rocks from the western Betics (S. Spain): Implications for crustal recycling in the lithospheric mantle beneath the westernmost Mediterranean: Lithos, v. 276, p. 45–61, https://doi.org/10.1016/j.lithos.2016.10.003.

von Bargen, N., and Waff, H.S., 1986, Permeabilities, interfacial areas and curvatures of partially molten systems: Results of numerical computations of equilibrium microstructures: Journal of Geophysical Research. Solid Earth, v. 91, p. 9261–9276, https://doi.org/10.1029/JB091iB09p09261.

Wang, K.L., O'Reilly, S.Y., Griffin, W.L., Pearson, N.J., and Zhang, M., 2009, Sulfides in mantle peridotites from Penghu Islands, Taiwan: Melt percolation, PGE fractionation, and the lithospheric evolution of the South China block: Geochimica et Cosmochimica Acta, v. 73, p. 4531–4557, https://doi.org/10.1016/j.gca.2009.04.030.

Wang, Z., Cheng, H., Zong, K., Geng, X., Liu, Y., Yang, J., Wu, F., Becker, H., Foley, S., and Wang, C.Y., 2020, Metasomatized lithospheric mantle for Mesozoic giant gold deposits in the North China craton: Geology, v. 48, p. 169–173, https://doi.org/10.1130/G46662.1.

Wasylenki, L.E., Baker, M.B., Kent, A.J., and Stolper, E.M., 2003, Near-solidus melting of the shallow upper mantle: Partial melting experiments on depleted peridotite: Journal of Petrology, v. 44, p. 1163–1191, https://doi.org/10.1093/petrology/44.7.1163.

Yaxley, G.M., Kamenetsky, V., Green, D.H., and Falloon, T.J., 1997, Glasses in mantle xenoliths from western Victoria, Australia, and their relevance to mantle processes: Earth and Planetary Science Letters, v. 148, p. 433–446, https://doi.org/10.1016/S0012-821X(97)00058-7.

Zelenski, M., Kamenetsky, V.S., Mavrogenes, J.A., Danyushevsky, L.V., Matveev, D., and Gurenko, A.A., 2017, Platinum-group elements and gold in sulfide melts from modern arc basalt (Tolbachik volcano, Kamchatka): Lithos, v. 290, p. 172–188, https://doi.org/10.1016/j.lithos.2017.08.012.

Science Editor: Brad S. Singer
Associate Editor: W.U. Reimold

Manuscript Received 29 January 2021
Revised Manuscript Received 5 July 2021
Manuscript Accepted 30 July 2021

Printed in the USA